Accepted Manuscript

Journal of the Geological Society

Sketch-Based Interface and Modelling of Stratigraphy and Structure in 3D

Carl Jacquemyn, Margaret E. H. Pataki, Gary J. Hampson, Matthew D. Jackson, Dmytro Petrovskyy, Sebastian Geiger, Clarissa C. Marques, Julio D. Machado Silva, Sicilia Judice, Fazilatur Rahman & Mario Costa Sousa

DOI: https://doi.org/10.1144/jgs2020-187

To access the most recent version of this article, please click the DOI URL in the line above. When citing this article please include the above DOI.

Received 1 October 2020
Revised 8 February 2021
Accepted 11 February 2021

Supplementary material at https://doi.org/10.6084/m9.figshare.c.5303043

Sketch-Based Interface and Modelling of Stratigraphy and Structure in 3D

Sketch-based geological modelling

Carl Jacquemyn[1]*, Margaret E. H. Pataki[1], Gary J. Hampson[1], Matthew D. Jackson[1], Dmytro Petrovskyy[2], Sebastian Geiger[2], Clarissa C. Marques[3*], Julio D. Machado Silva[3], Sicilia Judice[3], Fazilatur Rahman[3], Mario Costa Sousa[3]

[1]Imperial College London, UK.

[2]Heriot-Watt University, Edinburgh, UK.

[3]University of Calgary, Canada.

*present address: Computer Modelling Group Ltd., Canada

CJ: 0000-0002-8627-7144
GJH: 0000-0003-2047-8469
SG: 0000-0002-3792-1896

*Corresponding author: c.jacquemyn@imperial.ac.uk

Abstract

Geological modelling is widely used to predict resource potential in subsurface reservoirs. However, modelling is often slow, requires use of mathematical methods that are unfamiliar to many geoscientists and is implemented in expert software. We demonstrate here an alternative approach using Sketch-Based Interface and Modelling (SBIM) that allows rapid creation of complex three-dimensional (3D) models from 2D sketches. Sketches, either on vertical cross-sections or in map-view, are converted to 3D surfaces that outline geological interpretations. A suite of geological operators is proposed that handle interactions between the surfaces to form a geologically realistic 3D model. These operators deliver the flexibility to sketch a geological model in any order and provide an intuitive framework for geoscientists to rapidly create 3D models. Two case studies are presented, demonstrating scenarios in which different approaches to model sketching are used depending on the geological setting and available data. These case studies show the strengths of sketching with geological operators. Sketched 3D models can be queried visually or quantitatively to provide insights into heterogeneity distribution, facies connectivity or dynamic model behaviour; this information cannot be obtained by sketching in 2D or on paper.

Rapid Reservoir Modelling prototype (executable and source code) is available at: https://bitbucket.org/rapidreservoirmodelling/rrm . Supplementary screen recordings for the different case studies showing sketch-based modelling in action are available at https://doi.org/10.6084/m9.figshare.c.5084141

1 Introduction

Capturing geological heterogeneity is a key goal when constructing numerical models of the Earth's subsurface (e.g. Bentley, 2016; Boggs et al., 1992; Denver & Phillips, 1990; Hamilton & Jones, 1992; Jackson et al., 2013a; Jackson et al., 2015a; Jackson et al., 2005; Janković et al., 2006; Koltermann & Gorelick, 1996; Linde et al., 2015; Miller et al., 1998; Ronayne et al., 2008; Ronayne et al., 2010; White et al., 2004). Such models are used to predict the resource distribution and extraction potential of groundwater resources, geothermal reservoirs, oil and gas reservoirs, and ore deposits, as well as the behaviour of subsurface targets for nuclear waste or CO_2 storage (Deng et al., 2012; Geiger et al., 2009; Gershenzon et al., 2015; Graham et al., 2018; Ingebritsen et al., 2010; March et al., 2018; Matthäi et al., 2007; O'Sullivan et al., 2001; Sech et al., 2009; Shamshiri & Jafarpour, 2012; Sommer et al., 2013; Sun et al., 2008). However, the three-dimensional (3D) geometry and

spatial distribution of geological heterogeneity in the subsurface is uncertain, as boreholes sample only a small fraction of the rock volume and geophysical imaging methods lack the spatial resolution required to delineate all heterogeneities of interest (Feyen & Caers, 2006; Lemon & Jones, 2003; Linde et al., 2015; Ronayne et al., 2010). Expert knowledge is often used to predict the likely geometry and spatial distribution of heterogeneity away from boreholes, but geological interpretations are themselves subject to uncertainty. Numerical models based on different geological interpretations can yield highly varying predictions of system behaviour (e.g. Bentley & Smith, 2008; Bond et al., 2007; Brunetti et al., 2019; Deveugle et al., 2014; Refsgaard et al., 2012).

Even though geological models of the subsurface are very commonly used, current modelling tools often require specialist knowledge to capture the features of interest and are slow to create or update. Therefore they are not intuitive to use and are inaccessible to non-specialists or different disciplines. This is not ideal to quickly test an hypothesis or explore different geological concepts before starting a detailed modelling workflow. Here we will present a sketch-based approach that is intuitive to sketch geological models in 3D that is meant to rapidly capture geological ideas and concepts in 3D models. This enables us to communicate, learn, quantify or rank geology and its impact on flow in 3D.

Approaches to Computer Aided Design (CAD) and Computational Fluid Dynamics (CFD) outside of the geological modelling domain often include a significant element of prototyping: a number of simplified models are created to test different design concepts, before detailed models are created of the final agreed design (e.g. Arisoy & Kara, 2014; Cherlin et al., 2005; Shah et al., 2001). In geological modelling, analysis of different geological concepts is sometimes termed scenario testing, to differentiate it from the probabilistic modelling approaches that are used to create numerous model realizations around a single geological concept or scenario (Bentley & Smith, 2008). However, prototyping in geological modelling is rare, in part because there are no methods or software tools that allow rapid creation and testing of geological concepts. Most previous studies have instead focused on the development of methods and tools for probabilistic modelling around a single concept (e.g. Brunetti et al., 2019; Linde et al., 2015; MacDonald & Aasen, 1994; Strebelle, 2006; Yao et al., 2005).

Sketch-Based Interface and Modelling (SBIM) is an approach for rapid model creation that is used for prototyping in many non-geological CAD and CFD applications (e.g. Olsen et al., 2011; Olsen et al., 2009; Pereira et al., 2011). SBIM allows model concepts to be

rapidly sketched and tested. A number of studies have also proposed the use of SBIM in geological modelling (e.g. Amorim et al., 2012; Amorim et al., 2014; Jackson et al., 2015a; Lidal et al., 2013; Natali et al., 2014a; Natali et al., 2014b; Costa Sousa et al., 2020). SBIM in this context is based on the concept of using surfaces to capture geological architecture and heterogeneity (e.g. Denver & Phillips, 1990; Hamilton & Jones, 1992; Huysmans & Dassargues, 2011; MacDonald et al., 1998; White et al., 2004; Willis & White, 2000). The surfaces define and bound geological domains (Caumon et al., 2009; Jackson et al., 2013b; Jacquemyn et al., 2019; Pyrcz et al., 2005; Ruiu et al., 2016; Zhang et al., 2009). Surfaces may represent faults, fractures, stratigraphic surfaces, facies boundaries, lithological boundaries, diagenetic boundaries, and any other type of geological boundary (e.g. Caumon et al., 2009; Geiger et al., 2009; Graham et al., 2015; Jackson et al., 2015b; Jacquemyn et al., 2019; Massart et al., 2016a,b; Matthai et al., 2007; Pyrcz et al., 2005; Sech et al., 2009; White et al., 2004; Willis & White, 2000; Zhang et al., 2009). Geological domains, bounded by surfaces, can be defined without reference to an underlying grid or mesh (e.g. Jacquemyn et al., 2019), although a mesh may be created that conforms to the modelled surfaces when a numerical calculation is required (Jackson et al., 2015a; Zhang et al., 2018). The emphasis on surfaces and surface-bounded domains closely matches how geoscientists conceptualise and represent geological interpretations in traditional tools such as maps, cross-sections and block diagrams. The aim of SBIM here is not to simulate underlying geological processes, but to capture their effects on resulting geometries.

Previous applications of SBIM for geological modelling have been limited in their scope and applicability. Natali et al. (2014a, b) applied a SBIM methodology to sedimentary geology, with the goal of creating figures or animations for teaching or discussion. In their approach, geology must be sketched in depositional order, thus requiring that a geological history be interpreted prior to sketching. This is too restrictive for use as a prototyping SBIM tool, because it does not allow surfaces to be sketched in any order such that different concepts can be tested. Amorim et al. (2012) focused on interpretation of horizons from 3D seismic data using sketched surfaces. In contrast, Amorim et al. (2014) started with a blank screen and allowed the user to sketch lines, representing stratigraphic boundaries or faults, in map-view. The user sketched geological symbols onto the map which were used to control extrapolation of the sketched lines into 3D to form surfaces. Although both approaches constitute advanced examples of SBIM for geological application, they were too limited to be used for realistic geological modelling because, in their worked examples, the sketched

surfaces did not interact, and no operations were outlined for how interacting surfaces should be treated. Surface intersections in natural systems are ubiquitous, and a practical SBIM methodology for geology must have a robust and geologically intuitive approach to handle intersections. Furthermore, sketching only in map-view is too limited to replicate the geological architectures observed in natural systems. Geoscientists use sketches in both cross-section and map-view to capture these.

Here we report, for the first time, the use of SBIM to create 3D models of complex stratigraphy and structure, with direct relevance to rapid prototyping of subsurface reservoirs. We demonstrate application of our new SBIM approach using two typical example reservoir modelling scenarios, in which sketches are made at different scales, of different geological heterogeneity, and are constrained by different input data.

The SBIM methods presented here are implemented in an Open Source research code (Rapid Reservoir Modelling, RRM; Fig. 1; https://bitbucket.org/rapidreservoirmodelling/rrm) developed jointly by the authors that links a sketching interface with geological operators to build 3D models. The code also includes a flow diagnostics module to provide direct quantitative evaluation of such models. The aim of this paper is not to describe the numerical implementation in detail; a summary is provided, and other publications elsewhere describe the numerical algorithms and underpinning SBIM design concepts (Jackson et al., 2015a). Rather, we focus on how SBIM has been adapted and implemented for geological modelling, and on demonstrating its utility in rapidly testing different interpretations for subsurface reservoirs.

We first describe how 3D surfaces are created from 2D sketches and outline a suite of operators that control surface interactions such that the resulting sketched models are geologically realistic. In this first demonstration of SBIM for geological modelling, we explore its flexibility in stratigraphic and structural case studies. Both case studies illustrate scenarios that are common and important for subsurface reservoir characterization.

2 Methods

Our geological SBIM framework consists of two main components: a sketching component, that enables sketching on 2D planes from which 3D surfaces are generated, and a surface interaction component, that handles the intersections between the 3D surfaces and guarantees the representational validity of the sketched model. Screen recordings of the real-time sketching process and surface interactions for the models in this paper (Case studies I and II) are available in supplementary materials.

2.1 Creating 3D surfaces from 2D sketches

Geoscientists commonly create 2D sketches using pencil and paper. SBIM adopts the same approach but allows the geoscientist to create 2D sketches in a digital environment using an input device, such as a mouse or stylus, to draw directly on screen. Sketches are made in cross-section and/or map-view; however, the objective of SBIM as presented here is to create a 3D model. We have implemented three different approaches to create 3D surfaces from 2D sketches:

1. Sketch the intersection of the geological surface with one or multiple vertical 2D cross-sections and create a 3D surface by interpolation between the sketches.
2. Sketch depth and elevation contours on multiple horizontal 2D planes in map-view and create a 3D surface by interpolation between the sketches.
3. Sketch the intersection of the geological surface with a vertical 2D cross-section, and then sketch a trajectory in map-view. The cross-section is extruded along the trajectory to create a 3D surface.

2.2 Interactions of 3D surfaces

A key innovation in our geological SBIM approach is the definition of operators that dictate how sketched surfaces interact in 3D. These operators are based on fundamental geological rules for the interaction of stratigraphic surfaces that ensure any geological model is valid (Caumon et al., 2009; Jackson et al., 2005; White & Barton, 1999):

1. Surfaces cannot cross.
2. Surfaces cannot end within a domain.

3. Surfaces can either terminate against (truncate or conform) or remove (erode), existing surfaces.

The operators are designed to capture the relationships between stratigraphic surfaces that are required for model construction, but not to mimic geological processes. This is important because it allows the user to 'sketch what they see' without having to reproduce the underlying processes that created the observed stratigraphy. Moreover, it ensures that the operators are universally applicable to all stratigraphic settings and scales. The selected operator(s) are applied immediately after each new 3D surface is created, which means that surfaces do not need to be created in stratigraphic or hierarchical order. This is important for the prototyping applications we propose here, in which a complete geological interpretation may not be available at the onset of sketching; indeed, sketching and creation of 3D models may be a part of the interpretation process. The operators ensure that models contain watertight volumes (cf. Caumon et al., 2004) such that no gaps exist between truncating surfaces. We have identified two sets of operators, outlined below; visual representations of the operators are available in supplementary material S1 to S4, and screen recordings showing the use of operators in action are available in supplementary materials.

1. Operators that define how new sketched surfaces modify existing surfaces. The new sketched surface crops all or some of the existing surfaces.

    1.A 'Remove Above (RA)' – the RA operator removes the parts of any existing surfaces that lie above the new sketched surface. Existing surfaces that lie below the new sketched surface remain unchanged. A simple practical example of when this operator could be used is when sketching an erosional surface.

    1.B 'Remove Above Intersection (RAI)' – the RAI operator removes the parts of existing surfaces that are intersected by and lie above the new sketched surface. Existing surfaces that are not intersected by the new sketched surface remain unchanged. A simple practical example of when this operator could be used is when sketching an erosional surface after sketching overlying deposits.

    1.C 'Remove Below (RB)' – the RB operator removes the parts of any existing surfaces that lie below the new sketched surface. Existing surfaces that lie above the new sketched surface remain unchanged. A

simple practical example of when this operator could be used is when sketching basement contacts.

1.D 'Remove Below Intersection (RBI)' – the RBI operator removes the parts of existing surfaces that are intersected by and lie below the new sketched surface. Existing surfaces that are not intersected by the new sketched surface remain unchanged. A simple practical example of when this operator could be used is when sketching lateral accretion surfaces in a channel fill while removing previously interpreted channel-fill deposits.

2. Operators that set existing surfaces as boundaries for new sketched surfaces. The new sketched surface is cropped outside the assigned boundaries.

2.A 'Preserve Above (PA)' – The PA operator is applied to any existing surface such that it acts as a lower boundary for the next sketched surface. Only the parts of the new sketched surface that lie above this lower boundary are preserved and interact with existing surfaces. A simple practical example of when this operator could be used is when sketching strata that onlap or downlap onto an existing surface.

2.B 'Preserve Below (PB)' – The PB operator is applied to any existing surface, such that it acts as an upper boundary for the next sketched surface. Only the parts of the new sketched surface that lie below this upper boundary are preserved and interact with existing surfaces. A simple practical example of when this operator could be used is when sketching strata that underlie a previously sketched unconformity surface.

2.C 'Preserve Between (PBW)' – The PBW operator combines the PA and PB operators. Only the parts of a new sketched surface that lie above a selected lower boundary and below a selected upper boundary are preserved and interact with existing surfaces. A simple practical example of when this operator could be used is when sketching stratigraphic surfaces within a channel fill by preserving surfaces sketched between the channel-fill top and base, or adding further heterogeneity within layers and regions.

Operators can be combined, to provide the flexibility to sketch a model in any order, depending on data type, updating of data, and user preference: different users may favour a different order of sketching or interpretation. For example, some users may prefer to sketch hierarchically, starting with the large-scale features and progressively adding smaller-scale features. Some users may prefer to sketch in stratigraphic order, while others may sketch in no set order. All these approaches are possible in our SBIM implementation; irrespective of sketching order, the choice of appropriate operator allows the user to add or modify previously sketched surfaces, facilitating interpretation while sketching.

Stratigraphic surfaces are typically non-multivalued surfaces (ordinary or single-value surfaces), such that they do not recur in a vertical column unless deformed by later folding and faulting. Hence, the concepts of 'above' and 'below' can be unambiguously defined. This is not the case for multivalued surfaces resulting from deformation. Moreover, stratigraphic surfaces must be continuous across a model unless they terminate against another surface, whereas faults can end within a domain. Representing the full effects of faulting and folding is beyond the scope of this paper and is the subject of ongoing research. However, folding and faulting that does not result in multivalued surfaces can nonetheless be sketched using the current operators, so long as the fault surfaces do not end within the 3D model volume. We demonstrate preliminary application of SBIM for faulted reservoirs in case study II.

2.3 Numerical implementation

The details of the numerical implementation of the 2D sketching, 3D surface creation and sketch operators outlined above in our SBIM framework are beyond the scope of this geoscience-focused paper; instead, we provide a brief summary.

The 2D sketches are created using a sketching engine that implements well-established SBIM tools (see Olsen et al., 2009 for a review). The engine also implements some bespoke modifications required for our geological modelling application, including (i) vertical exaggeration while sketching, to account for the very high aspect ratio of most geological models, and (ii) the ability to sketch over data in a given sketch plane, such as borehole data, seismic data or outcrop images, as demonstrated in our example applications.

The sketches are converted to a set of points defined in Cartesian space. The point data, which may have been created from multiple sketches on different cross-sections, are then passed to the surface modelling engine which creates a 3D surface from the data in one of two ways. In the first approach, the surface is created by interpolation using thin-plate

splines (Duchon, 1977) as kernels for surface reconstruction. Overfitting is avoided by reconstructing surfaces using approximate interpolation (Wendland & Rieger, 2005), which finds the surfaces that best fit the sketch data within a prescribed margin of error. The balance between accuracy and stability in surface reconstruction is mediated by the resolution of the model being built and the complexity of the 3D surface. As with any interpolation-based surface reconstruction, the resulting surfaces may not preserve geological realism away from the sketched data. Further sketches can be added to constrain the surface reconstruction if needed.

The second approach can better preserve geological realism by extruding a cross-section sketch along a trajectory sketched in map-view. The extrusion method depends on the geometry of the cross-section and trajectory. If the curvature of the guiding trajectory is small enough that a cross-section can be extruded along it without the resulting surface intersecting with itself, then an actual extrusion is computed by interpolating the cross-section and trajectory independently and creating a surface given as a tensorial product of the input curves. To account for the more general case in which a cross-section extruded along a trajectory may self-intersect, the use of a tensorial product is excluded. In this case, the cross-section is guided using a vector field that coincides with the trajectory's tangent vectors at the trajectory location. To minimise distortion it is required that the vector field is divergence-free and that the vectors' magnitudes near the trajectory are close to one; these restrictions are enforced by using matrix-valued conditionally positive definite functions as kernels for the vector-field interpolation (Narcowich & Ward, 1994). A vector-field is required that must be integrated while ensuring it is finely sampled where the guided surface has high gradient, and this more general approach for extrusion is thus more CPU intensive than using the tensorial product of cross-section and trajectory.

Once a new 3D surface is created, it is passed to the operator engine. Consistent and efficient implementation of the operators described in the previous section has been one of the most challenging aspects of our numerical implementation of SBIM. In essence, the operators are mapped onto an order-theoretic lattice defined on continuous surfaces to represent the geological models. The operator engine continuously determines surface intersections and performs additional queries, such as ordering the surfaces according to the relative geological age defined by surface interactions. Efficient implementation means that the computational cost of the operator engine scales linearly with the number of surfaces in a model.

3 Results

3.1 Case study I: Shallow marine strata – well correlation

3.1.1. Context and geological setting

Reservoirs deposited in shallow-marine environments are important groundwater resources in many areas of the world (e.g. Fahad Al-Ajmi et al., 2015; Huysmans et al., 2008; Mayo et al., 2003; Taylor et al., 2001) as well as oil and gas reservoirs and targets for geological CO_2 storage (e.g. Ashraf et al., 2013; Jackson et al., 2009; Sech et al., 2009). However, stratigraphic sections can be correlated between boreholes in a variety of ways, depending on the number and spacing of boreholes, the data types available to constrain the correlation and the depositional concept(s) applied. The aim of the modelling in this case study is to test the impact of different borehole correlations and depositional concepts on 3D facies architecture in marginal-marine and shallow-marine strata of the Spring Canyon Member, Blackhawk Formation in the Book Cliffs, Utah, USA. The Spring Canyon Member is interpreted as a series of vertically stacked, regressive-transgressive tongues (parasequences) that were deposited by wave-dominated deltas and laterally adjacent strandplains during regression and wave-dominated, tide-influenced barrier island systems (containing tidal inlets and flood tidal deltas) during transgression (Campion et al., 2010; Hampson & Howell, 2005; Kamola & Van Wagoner, 1995).

We use SBIM to create the 3D models, honouring data from five measured outcrop sections and boreholes (Fig. 1) (Campion et al., 2010; Kamola & Van Wagoner, 1995). These data and associated outcrops are widely used in education and training to develop geological interpretation skills, but their educational value can be significantly enhanced by translating the correlation panel between measured outcrop sections and boreholes into 3D models that demonstrate the impact of different interpretations on predicted aquifer or reservoir character and behaviour. SBIM allows this in a rapid and intuitive manner and could be executed in the field using tablets equipped with touch-sensitive screens. The data used here were vertically exaggerated by a factor of 150 and we chose to sketch in this aspect ratio, but the resulting models can easily be rescaled to true aspect ratio for quantitative calculations.

Variations exist in how interpreted sequence stratigraphic surfaces, facies belts and geobodies can be correlated between the boreholes, and in the map-view geometry of the surfaces, belts and geobodies. The following five interpretation scenarios are explored. These scenarios represent different interpretations of stratigraphic architecture in regions that lie

between the outcrop sections and boreholes in the 2D cross-section, and variations in 3D stratigraphic architecture away from the cross-section. The scenarios tested are as follows:

Scenario SM1: Initial interpretation

Scenario SM2: Variation of down-dip extent of shoreface facies belts (as recorded by sketched cross-section relationships)

Scenario SM3: Variation of shoreline orientation and rugosity (as recorded by sketched map-view trajectory)

Scenario SM4: Variation of the extent and geometry of flood tidal delta deposits (as recorded by sketched cross-section relationships and map-view trajectory)

Scenario SM5: Variation of the extent and geometry of tide-influenced channelised sandbodies (as recorded by sketched cross-section relationships and map-view trajectory).

These scenarios are broadly consistent with previously published interpretations but differ in their detail to show the flexibility of SBIM to prototype 3D interpretations and rapidly create 3D geological models from sparse datasets.

3.1.2. Initial interpretation scenario SM1

The initial interpretation (SM1; Fig. 2) consists of three parasequences separated by sketched flooding surfaces. Each parasequence is subdivided into facies belts by sketched facies-bounding surfaces, consistent with the outcrop sections and borehole data (Fig. 1). The middle parasequence contains a flood tidal delta, consistent with observations at the Sowbelly Gulch section (Fig. 1), and this is captured by sketching surfaces that represent the top and base of the flood tidal delta deposits, which are considered to form a continuous facies belt in this initial interpretation. The upper parasequence contains a tide-influenced channelised sandbody, consistent with observations at the Gentile Wash section (Fig. 1), and this is captured by sketching surfaces that represent the top and base of the sandbody. In this initial interpretation, the channelised sandbody has been interpreted to comprise a single, tide-influenced deltaic distributary channel that was active during regression of a nearly linear shoreface and associated strandplain. The cross-section view in Fig. 2 (top) shows the vertical (2D) sketched correlation. However, in the subsurface, the 3D geometry of the parasequences, facies belts and tidal deposits could not be deduced from the available data;

even in this outcrop section, the relative lack of 3D control means there is significant uncertainty.

Here, we exploit the convenience and speed of SBIM to extend the 2D correlation into 3D, based on conceptual understanding of the depositional system. We extrude each surface sketched in cross-section along a trajectory sketched in map-view (Fig. 2, bottom right). We assume a close-to-linear shoreline in this initial interpretation. The trajectories sketched for the parasequence-bounding flooding surfaces represent the interpreted shoreline palaeogeography of each parasequence; these trajectories are re-used for the facies-bounding surfaces, consistent with the interpretation that the facies belts, including the flood-tidal delta deposits, are continuous in the shoreline-parallel direction. Also shown is the sketched trajectory of the tide-influenced channelised sandbody (red), which corresponds to the channel thalweg and is interpreted to be oriented approximately perpendicular to the shoreline. The 3D perspective view in Fig. 2 (bottom left) shows the resulting 3D model, created entirely using SBIM. SM1 is the only scenario that needed to be sketched from 'blank screen'; the other scenarios all modify this initial 3D model, as outlined below.

The sketching workflow for this example simply involves sketching the correlation on the cross-section view (top) and adding a map-view trajectory. All boundaries (flooding surfaces, facies boundaries) are sketched in a single E-W cross-section, except for the boundary of the tide-influenced channelised sandbody, which is sketched in a N-S cross-section.

We initially choose to sketch in hierarchical order, from the largest to the smallest scale. Each 2D sketch is extruded along the associated sketched trajectory to create a 3D surface before the next surface is sketched; we focus here on how the surfaces are sketched in cross-section. The parasequence boundaries (flooding surfaces) are sketched first from base to top, using operator RA or RAI to remove overlapping portions of earlier sketched surfaces (surfaces 1-3 in Fig. 3a; screen recording available in supplementary materials). Next, we add the surfaces denoting the boundaries between facies belts, using the operator PBW to ensure the sketched surfaces are truncated against the parasequence-bounding surfaces.

In the lower parasequence, the PBW operator is activated between its bounding flooding surfaces, and facies boundaries are sketched from bottom to top using operator RA or RAI (surfaces 5-9 in Fig. 3b). In the middle parasequence, the lowest three facies boundaries are also sketched from bottom to top combining PBW with RA or RAI (surfaces

11-13 in Fig. 3c). Next, the flood tidal delta is sketched, again using operator RA or RAI (surface 14 in Fig. 3c). A new sketching region within which to apply PBW is then selected above the flood tidal delta and below the upper parasequence boundary (Fig. 3c). The final two facies boundaries are then sketched within this region using RA/RAI (surfaces 16-17 in Fig. 3c), with use of PBW ensuring they terminate against the top of the flood tidal delta.

In the upper parasequence, the lower three facies boundaries are sketched from bottom to top using RA/RAI, followed by the upper facies boundary (surface 22 in Fig. 3d). This latter surface also represents the top of the channelised sandbody; the operator PB is applied to this surface and the channelised sandbody is sketched using operator RA/RAI: the resulting erosional channel base truncates earlier sketched surfaces but is itself truncated against the channel top surface (surface 27 in Fig. 3d). A new sketching region within which to apply PBW is then chosen, below the base of the channelised sandbody and above the underlying facies boundary. The final two facies boundaries are then sketched in this region using operator RA/RAI.

The sketching approach described above is just one of many that can be followed to create the initial interpretation model and we show three alternative approaches that yield the same final 3D model in Fig. 3. It is this flexibility in sketching approaches that makes SBIM combined with geological operators so powerful. In general, when sketching surfaces in order from bottom to top, the operators RA and RAI are commonly used (e.g. Fig. 3e-h). The same outcome can be achieved when sketching from top to bottom using operators RB and RBI (e.g. Fig. 3i-l). PBW is a useful operator when sketching in hierarchical order, as surfaces at lower levels of the hierarchy can be constrained to lie within surfaces at higher levels. However, there is no need to sketch in hierarchical order. Some users might prefer to sketch in stratigraphic order (e.g. Fig. 3 e-h). Some may prefer to sketch in any order, with no regard to hierarchy or stratigraphy (e.g. Fig. 3 m-p). Regardless of the approach used, the 3D model can be created in less than 10 minutes.

Perspective views of different parts of the initial interpretation model (Fig. 4) show the spatial relationships and connectivity of facies belts and geobodies in 3D. Every parasequence consists of a repeated pattern (Fig. 4a-c-f), with facies belts stacked vertically and laterally from offshore transition (grey) in the deepest and most distal position (East) overlain by lower shoreface (distal: brown; proximal: orange), upper shoreface and foreshore (yellow - pale yellow) to coastal plain facies (green) in the shallowest and most proximal

position (West). The linear belt of flood tidal delta deposits in the middle parasequence (Fig. 4 d-e) lies at the up-dip termination of the foreshore and upper shoreface facies belts.

Offshore transition (grey) and coastal plain (green) facies are predominantly composed of very low-permeability mudstones, and may form significant aquitards or barriers where they are laterally extensive and continuous. Conversely, upper shoreface (yellow), foreshore (pale yellow), channel-fill and flood-tidal delta (red) facies are high-permeability sandstones, with best aquifer or reservoir potential. As a result, each parasequence is composed of an aquifer/reservoir in its upper part and an aquitard/barrier in its lower part. Parasequences pinch out to the west (palaeo-landward) into a coastal plain aquitard. In this initial interpretation, the lateral continuity of offshore transition aquitards limits the vertical connectivity of aquifer sandstones in each parasequence, with hydraulic communication only possible through heterolithic distal lower shoreface facies (brown) and low-permeability proximal lower shoreface facies (orange). The large dip extent of shoreface facies belts and strike continuity of flood-tidal delta facies in this initial model results in large aquifer volume and high lateral aquifer continuity (Fig. 4d-e). The channelised sandbody in the upper parasequence increases aquifer/reservoir volume and local lateral continuity, and provides the potential to locally erode through the lower part of the parasequence, thus providing vertical connectivity with aquifer sandstones in the underlying parasequence (Fig. 4b).

3.1.3. Alternative interpretation scenarios

Unlike this outcrop example, subsurface datasets typically contain insufficient information to constrain the dip extent of facies belts between boreholes, and this is an important uncertainty to consider. In scenario SM2, the down-dip extents of shoreface facies belts are modified, which results in a different parasequence stacking pattern (Fig. 5a-b). The initial model exhibited a progradational-to-aggradational parasequence stacking pattern (Kamola & Huntoon, 1995), whereas this second scenario reflects a uniformly aggradational stacking pattern (Fig. 5b).

Depending on the sketching order used to create the initial model SM1, the sketched parasequence bounding surfaces can be re-used, simply by undoing sketches of facies bounding surfaces (steps 4-20 in procedure #1 of Fig. 3a-d) before sketching the new surfaces. Alternatively, a combination of PA and PB can be used to select, respectively, the base and top bounding surface of a parasequence, and RA or RB used to remove all facies

bounding surfaces within the selected parasequence before sketching the new surfaces. The sketching process for this second scenario is then identical to that used for the initial interpretation model, including re-use of the same plan-view trajectories (screen recording available in supplementary materials), except that we vary the sketches of the facies-belt boundaries so that their down-dip terminations occur in different locations compared to SM1.

The modelled dip extent of facies belts has a quantifiable impact on relative facies proportions (Fig. 5b), representing a reduced extent and volume of aquifer sandstones in each parasequence. Offshore transition and coastal plain aquitards retain their lateral extent and continuity, such that aquifers remain poorly connected vertically.

Scenario SM3 explores variations in the map-view trajectory of shoreface facies belts, which reflects shoreline orientation and rugosity (Fig. 5 c-d). The cross-sectional correlation between the measured outcrop sections and boreholes is maintained from the initial model SM1, but the orientation and rugosity of shoreface facies belts in each parasequence is sketched using a different map-view trajectory. The same trajectory is used for the upper bounding surface of each parasequence and the facies-bounding surfaces within that parasequence. Here we modify the map-view trajectories for all three parasequences. However, an individual parasequence could be modified while the others remain unchanged. The sketching process for SM3 is identical to the initial interpretation, differing only in the map-view trajectories used (screen recording available in supplementary materials).

The facies proportions in model SM3 change only marginally relative to the initial model SM1 (Fig. 5d), but the distribution of high-quality aquifer sandstones is modified in each parasequence. The area of foreshore and upper shoreface sandstones that are overlain by coastal plain mudstones at the top of the middle parasequence is increased (Fig. 5d), such that the vertical connectivity between these sandstones and overlying low-quality proximal lower shoreface sandstones in the upper parasequence is decreased.

In scenario SM4, a different geometry is considered for the flood tidal delta deposits in the middle parasequence (Fig. 5 e-f). In the previous scenarios, these deposits were interpreted as a linear facies belt aligned parallel to the shoreface (Fig. 2). In scenario SM4, the flood tidal delta deposits are instead interpreted as landward protruding lobes that extend from the shoreface (Hampson & Howell, 2005). The sketching procedure is identical to SM1, except a different approach is used to sketch the lobate geometry of the flood tidal delta deposits. The top of each flood tidal delta is constructed by sketching contours on horizontal

planes, one at the top of the delta and one at the base of the delta (Fig. 6 a&c). An additional sketching plane can be added in the middle for extra control on the final geometry (Fig. 6b).

The sketching process is shown in supplementary screen recordings, starting from the initial interpretation, removing the middle and upper parasequence and finally sketching the new geometry for the flood tidal delta deposits. The SBIM approach is, however, sufficiently flexible to allow an alternative approach, in which these surfaces are sketched in multiple vertical cross-sections, either in dip section or strike section (Fig. 6 d-f). For example, on strike-parallel cross-sections, one sketch to delineate the highest point (Fig. 6e), and two cross-sections at the distal and proximal termination (Fig. 6 d&f) are sufficient to generate the top surface of the delta.

Facies proportions in model SM4 (Fig. 5f) change slightly from those of the initial model, with an increased proportion of coastal plain facies and a reduced up-dip extent and volume of high-quality aquifer sandstones in the middle parasequence. This results in a reduced volume and less continuous distribution of high-quality flood-tidal delta sandstones that are no longer connected.

Finally, scenario SM5 tests a different interpretation of the tide-influenced channelised sandbody that cuts into the top of the upper parasequence (Fig. 5g-h). In scenario SM5, the sandbody is instead interpreted to form part of a tide-influenced deltaic distributary channel network (Fig. 5h); the geometry of the underlying shoreline and shoreface facies belts are also modified to represent the arcuate geometry of a wave-dominated delta rather than a linear strandplain. To sketch scenario SM5 from the initial interpretation, the upper parasequence is removed (undo last 8 sketched surfaces) and a new version sketched. In this example, the same order of sketching is used as in SM1. The curved geometry of the shoreface facies belts in the upper parasequence is constructed simply by using a different map-view trajectory. The distributary channel network is sketched as contours on two horizontal planes, one for the channel bases and one for the channel tops. A screen recording shows the sketching workflow for this model (screen recording available in supplementary materials).

Facies proportions in model SM5 vary slightly from the initial interpretation SM1 (Fig. 5h), with an increased proportion of tide-influenced channel-fill deposits. The area of proximal lower shoreface sandstones in the upper parasequence that overlie foreshore and upper shoreface sandstones at the top of the middle parasequence is reduced, such that the

vertical connectivity between these sandstones is decreased. Increased volume of channelised sandbodies in the upper parasequence enhances their potential to locally erode through the lower part of this parasequence, and thus provide vertical connectivity with the aquifer sandstones in the middle parasequence.

3.2 Case study II: Normal fault array – outcrop cross-section

3.2.1. Context and geological setting

It is well known that faults can significantly affect fluid flow in aquifers and reservoirs, and impact seal integrity for CO_2 storage (e.g. Aydin, 2000; Bense & Person, 2006; Dockrill & Shipton, 2010; Frery et al., 2015). In this second case study, we demonstrate that faults can also be captured in a 3D model using SBIM (Fig. 7). The case study models faulted, interbedded sandstones, mudstones and limestones in an exposed part of the footwall damage zone of the Moab Fault (Doelling et al., 2002; Foxford et al., 1996). The exposure contains an array of normal faults in a nearly vertical road cut next to Highway 191, opposite the main entrance to Arches National Park, Utah, USA. The beds in this outcrop belong to the upper part of the Honaker Trail Formation (Late Pennsylvanian), deposited in shallow marine shelf and nearshore environments (Doelling et al., 2002).

The aim of the modelling is to test different fault configurations that are prominent at the scale of the outcrop (110 x 40 m), ignoring smaller scale fractures and deformation bands. Faults in this outcrop (Fig. 7) show a synthetic or antithetic orientation relative to the main Moab Fault (Torabi et al., 2019).

We use SBIM to delineate bed boundaries (from bottom to top: purple-red-yellow-green) as well as faults (west-dipping: dark blue; east-dipping: light blue) by sketching over the outcrop photograph (Fig. 7 top). Although the features in this outcrop are easy to recognise, there is uncertainty in how the faults may be interpreted and modelled away from the outcrop face, and we use SBIM to rapidly create 3D models that explore and test different scenarios. In some of these scenarios, we deviate from the published interpretation (Torabi et al., 2019), in order to demonstrate the flexibility of the SBIM approach, sketching a conjugate fault set in which antithetic faults exhibit a different strike orientation relative to the main Moab Fault. The scenarios tested are as follows:

Scenario NF1: Initial interpretation; antithetic faults with strike parallel to Moab fault

Scenario NF2: Antithetic faults forming intersecting conjugate fault sets

Scenario NF3: Antithetic faults forming intersecting conjugate fault sets with two additional fault blocks.

3.2.2. Initial interpretation scenario NF1

In the initial interpretation model, strike-parallel synthetic and antithetic faults are sketched (respectively dark and light blue in Fig. 7), as reported by Torabi et al. (2019). The plane of the outcrop face is assumed to be oriented perpendicular to the strike direction of all faults.

This initial model is constructed by first sketching all the faults, and then sketching the bed boundaries within each fault block, in the outcrop cross-section (Fig. 8a-d). Sketching of the faults can begin with any fault (Fig. 8a-b). For each fault, the sketching operator to apply depends on whether it is in the footwall or hanging wall of previously sketched faults. When sketching a new fault in the footwall of a previously sketched fault, RB or RBI is most appropriate. When sketching a new fault in the hanging wall of a previously sketched fault, RA or RAI is most appropriate. Alternatively, PBW can be used to select two faults and sketch within all fault blocks that they bound. Sketching the bed boundaries within a fault block also relies on PBW, to constrain the boundaries within the selected block (Fig. 8c-d). Within a fault block, bed boundaries can be added in any order, similar to case study I (Fig. 3). A step-by-step screen recording of this sketching approach is available in supplementary materials.

An alternative approach is to mix sketching of stratigraphy and faults (Fig. 8 e-h). Some bed boundaries are sketched first (Fig. 8e), and are subsequently truncated by a sketched fault (Fig. 8f). If the sketched bed boundaries lie in the footwall of the new fault surface, the RA or RAI operator is used to truncate the bed boundaries correctly, and RB or RBI if the previously sketched boundaries lie in the hanging wall. This will generate two fault blocks, one with bed boundaries already sketched, and another fault block that is empty. Bed boundaries (or additional faults) are then sketched within the empty fault blocks (Fig. 8g-h). The combination of sketch operators allows faults and fault blocks to be added after stratigraphy has been sketched.

Once a fault or bed boundary has been sketched in the outcrop cross-section (Fig. 8), it is then extruded perpendicular to the sketching plane, from front to back of the model. Consequently, all cross-sections parallel to the outcrop face are identical (Fig. 9a-c). The perspective views in Fig. 9 show how the continuity of some beds is affected by faulting. Assuming that transmissibility of the faults is not impacted by clay smear or cementation (i.e. there is no membrane sealing), most beds are still connected across most faults. However, in

this initial interpretation model, no connectivity is preserved with the westernmost fault block (highlighted by the blue rectangle in Fig. 9b). Thinner beds (e.g. yellow bed in Fig. 9a) are generally disconnected. If these thin beds were conduits to flow, the faults would create flow barriers by juxtaposition sealing. Conversely, if the thin beds were barriers to flow, the faults would disconnect them laterally such that they form baffles around which fluids can pass.

3.2.3. Alternative interpretation scenarios

In scenario NF2 (Fig. 9 d-f), different strike orientations are sketched for the faults interpreted as synthetic (Fig. 7; dark blue) and antithetic (Fig. 7; light blue) to represent intersecting conjugate fault sets. In the outcrop cross-section, the interpretation does not change and the sketching workflows in Fig. 8 is applied, but the synthetic faults are extruded along a NNW-SSE trajectory, whereas the antithetic faults are extruded along a NNE-SSW trajectory. The 3D geometry of the model shows the more complex relationships between fault blocks (Fig. 9d-f). The differences in fault orientation are most obvious in the lowest beds of the model (Fig. 9e). An important difference between this scenario and scenario NF1 is visible on the right-hand (NW) corner of the model (Fig. 9e; highlighted by blue dashed square), where the geometry of the fault block is changed and yellow and light green beds are exposed, in contrast to the initial model (Fig. 9b; highlighted by blue dashed square). Because the model is no longer a perpendicular extrusion of the sketched cross-section, not every volume is intersected and visible in a single cross-section. Moving to different cross-sections towards the front or back of the model exposes the lack of some beds, which must be sketched on different cross-sections. A step-by-step sketching video is available in supplementary materials.

The change in strike of the faults to a conjugate set rather than parallel faults has an impact on bed connectivity. In comparison to scenario NF1, most beds remain connected from west to east, but now also including connectivity with the westernmost fault block (Fig. 9b,e; highlighted by blue dashed square); here, the orange bed is only just connected with the westernmost fault block. East-west fluid flow through the orange bed would be possible in this scenario. There is no change in connectivity of the thin beds, as they are not juxtaposed across any fault.

In scenario NF3 (Fig. 9 g-i) additional fault blocks are modelled by sketching additional antithetic faults in model NF2 (highlighted by the blue arrows in Fig. 9d,g and blue circles in Fig. 9f,i). Because the newly sketched faults and fault blocks do not intersect the

outcrop cross-section, this is an equally possible scenario as NF2. To sketch the additional fault blocks, PBW is used to constrain new sketched fault surfaces within an existing fault block(s). RA or RB is used depending whether the existing bed boundaries or faults are respectively in the footwall or hanging wall of the new sketched fault. The existing fault blocks are truncated by this new fault, and new bed boundaries are sketched within the footwall of the new fault (steps 37-42 in workflow #2 of Fig. 8h). Structure and stratigraphy do not have to be sketched in a prescribed order but can be sketched in different combinations. Adding a new fault and sketching bed boundaries inside the new fault block was completed in less than four minutes. A step-by-step sketching video is available in supplementary materials.

The addition of two new antithetic faults has no impact on the connectivity of thicker beds (e.g. red and orange beds in Fig. 9 h & i are still connected). However, the additional faults have caused further disconnection of thin beds (e.g. yellow bed highlighted by the blue arrow in Fig. 9d,g).

4 Discussion

Our new SBIM modelling approach allows, for the first time, geoscientists to create 3D geological models using an intuitive approach that is similar to sketching in 2D on paper. Such sketches are familiar to geoscientists as they are often used to conceptualise and communicate geology in maps, cross-sections and block diagrams. Our geological operators allow surfaces to be sketched in any order so geoscientists can interpret as they sketch, prototyping geological concepts and testing alternative conceptual models and scenarios. 3D models can be created very rapidly compared to most currently available expert software and with minimal training. Sketching a model from blank screen typically takes minutes to tens of minutes, and models can be sketched in the field using tablets with touch sensitive screens, as well as in the office.

The resulting models are quantitative and, although a detailed description of such calculations lies outside the scope of this paper, the models can be used to determine key aquifer and reservoir properties. Volumetric calculations, such as total or connected volumes and fluid storage capacity of a given facies, can be obtained directly from the sketched model. However, we have also integrated our implementation of SBIM for 3D reservoir modelling with computationally cheap flow diagnostics. Such flow diagnostics allow key flow properties and behaviour to be assessed using a single pressure solution (Zhang et al.,

2017; Zhang et al., 2020). Together, SBIM and flow diagnostics allow rapid, quantitative assessment of the impact of different geological concepts and scenarios on resource volumes and flow properties. Fig. 10 shows an example of our flow diagnostics module in action on sketched model SM5. Here, the pressure field obtained for a given combination of injection and offtake boreholes allows the fluid 'time of flight' to be calculated, highlighting key flow paths through connected aquifer facies. Petrophysical properties are assigned to facies or other geologically defined rock units using a simple interface, and boreholes can be interactively added and moved around the model with flow properties updated essentially instantaneously.

Comparison of sketch-based modelling, as implemented here, to other modelling tools reveals a number of advantages and disadvantages. The advantages of sketch-based modelling include ease of use and flexibility in the features that can be modelled. Sketching a geological model is intuitive: it does not require users to learn complicated workflows and their underlying methods. The operators introduced here allow users to sketch surfaces in any order, rather than being forced to follow stratigraphic ordering, a length-scale based hierarchy, or order imposed by a pre-defined workflow. Intricate geometries, which are hard to replicate using existing modelling approaches, can be sketched in 3D. The disadvantages of sketch-based modelling are inherent to its design as a propotyping tool. Despite its capability to generate models quickly, sketch-based modelling is not designed to generate hundreds or thousands of realisations of the same base case as in conventional stochastic modelling tools and workflows, but rather to explore scenarios that are conceptually different. We emphasize that our aim is not to replace conventional workflows, but rather to complement them. Finally, sketching is easiest on touchscreen-enabled devices, such as laptops and tablets, either using a stylus or fingers. Sketching with a computer mouse is less natural and requires the user to find a balance between precision and speed.

Potential applications of our implementation of SBIM for 3D geological modelling are numerous and include characterization of subsurface groundwater and hydrocarbon resources and potential sites for CO_2 storage. There are also broad potential applications in geoscience education and training. 3D models can easily be sketched in the classroom or the field, so that qualitative observations and quantitative calculations can be assessed directly and communicated with peers. The quick turnaround time from conceptual sketch to model output encourages geological thinking in 3D, and integration with flow diagnostics demonstrates the impact of geological interpretation on predicting subsurface flow behaviour.

The current set of geological operators are sufficiently robust for any stratigraphic model and a range of simple structural scenarios. Ongoing development of RRM is focused on extending the sketching of structure to include more complex scenarios including faults that tip-out within the model domain, and on further simplifying the user experience, for example by allowing users to edit existing models and sketch template surfaces that can be re-used to avoid repetitive sketching. We are also expanding the geological operators to allow a wider range of structural settings and diagenetic alteration to be modelled.

5 Conclusions

In this paper we present the first application of sketch-based interface and modelling (SBIM) for rapid and intuitive creation of realistic 3D geological models. We integrate SBIM with geological operators to allow a flexible approach to sketching. The result is a fast, geologically robust prototyping tool that leverages traditional techniques to conceptualise geological interpretations such as maps, cross-sections and block diagrams, without requiring specialist modelling expertise. The resulting models can be assessed visually and their volumetric properties and dynamic flow behaviour evaluated quantitatively. In addition to a wide range of applications for resource estimation, there are educational benefits of our modelling approach in developing 3D geological interpretation and visualisation skills.

6 Acknowledgments

The authors want to thank the members of Phase 1 of the Rapid Reservoir Modelling Consortium (Equinor, ExxonMobil, Petrobras, Shell and IBM Research Brazil/IBM Centre for Advanced Studies, Alberta, Canada) and Phase 2 of the Rapid Reservoir Modelling Consortium (Equinor, ExxonMobil, Petrobras, Petronas and Shell) for funding this work and granting permission to publish this paper. Geiger acknowledges partial funding for his Chair from Energi Simulation. The authors thank Subject Editor Sarah Boulton, reviewer Tore Grane Klausen and an anonymous reviewer for their insightful and constructive comments on the manuscript.

7 References

Amorim, R., Brazil, E. V., Patel, D., & Costa Sousa, M. (2012). *Sketch modeling of seismic horizons from uncertainty*. Paper presented at the EUROGRAPHICS symposium on sketch-based interfaces and modeling.

Amorim, R., Brazil, E. V., Samavati, F., & Costa Sousa, M. (2014). *3D geological modeling using sketches and annotations from geologic maps*. Paper presented at the Proceedings of the 4th Joint Symposium on Computational Aesthetics, Non-Photorealistic Animation and Rendering, and Sketch-Based Interfaces and Modeling, Vancouver, British Columbia, Canada.

Arisoy, E. B., & Kara, L. B. (2014). *Topology preserving digitization of physical prototypes using deformable subdivision models*. Paper presented at the ASME 2014 International Design Engineering Technical Conferences and Computers and Information in Engineering Conference.

Ashraf, M., Oladyshkin, S., & Nowak, W. (2013). Geological storage of CO_2: Application, feasibility and efficiency of global sensitivity analysis and risk assessment using the arbitrary polynomial chaos. *International Journal of Greenhouse Gas Control, 19*, 704-719. https://doi.org/10.1016/j.ijggc.2013.03.023

Aydin, A. (2000). Fractures, faults, and hydrocarbon entrapment, migration and flow. *Marine and Petroleum Geology, 17*(7), 797-814. https://doi.org/10.1016/S0264-8172(00)00020-9

Bense, V. F., & Person, M. A. (2006). Faults as conduit-barrier systems to fluid flow in siliciclastic sedimentary aquifers. *Water Resources Research, 42*(5). https://doi.org/10.1029/2005wr004480

Bentley, M. (2016). Modelling for comfort? *Petroleum Geoscience, 22*(1), 3-10. https://doi.org/10.1144/petgeo2014-089

Bentley, M., & Smith, S. (2008). Scenario-based reservoir modelling: the need for more determinism and less anchoring. *Geological Society, London, Special Publications, 309*(1), 145-159. https://doi.org/10.1144/sp309.11

Boggs, J. M., Young, S. C., Beard, L. M., Gelhar, L. W., Rehfeldt, K. R., & Adams, E. E. (1992). Field study of dispersion in a heterogeneous aquifer: 1. Overview and site description. *Water Resources Research, 28*(12), 3281-3291. https://doi.org/10.1029/92wr01756

Bond, C. E., Gibbs, A. D., Shipton, Z. K., & Jones, S. (2007). What do you think this is? "Conceptual uncertainty" in geoscience interpretation. *GSA today, 17*(11), 4. https://doi.org/10.1130/GSAT01711A.1

Brunetti, C., Bianchi, M., Pirot, G., & Linde, N. (2019). Hydrogeological model selection among complex spatial priors. *Water Resources Research, 55*(8), 6729-6753. https://doi.org/10.1029/2019wr024840

Campion, K. M., Van Wagoner, J. C., Mitchum, R. M., Rahmanian, V. D., & Kalbas, J. L. (2010). Excercise 2.1 - Parasequence associations in a shoreline succession: Blackhawk Formation, near Helper, Utah. In V. Abreu, J. E. Neal, K. M. Bohacs, & J. L. Kalbas (Eds.), *Sequence Stratigraphy of Siliciclastic Systems – the ExxonMobil Methodology: SEPM, Concepts in Sedimentology and Paleontology* (Vol. 9, pp. 19-29): SEPM.

Caumon, G., Collon-Drouaillet, P., Le Carlier de Veslud, C., Viseur, S., & Sausse, J. (2009). Surface-based 3D modeling of geological structures. *Mathematical Geosciences, 41*(8), 927-945. journal article. https://doi.org/10.1007/s11004-009-9244-2

Caumon, G., Lepage, F., Sword, C. H., & Mallet, J.-L. (2004). Building and editing a sealed geological model. *Mathematical Geology, 36*(4), 405-424. https://doi.org/10.1023/B:MATG.0000029297.18098.8a

Cherlin, J. J., Samavati, F., Costa Sousa, M., & Jorge, J. A. (2005). *Sketch-based modeling with few strokes*. Paper presented at the Proceedings of the 21st Spring Conference on Computer Graphics, Budmerice, Slovakia. https://doi.org/10.1145/1090122.1090145

Costa Sousa, M.. Machado Silva, J.D., Marques, C.C., Moura De Carvalho, F., Judice, S., Rahman, F., Jacquemyn, C., Pataki, M.E.H., Hampson, G.J., Jackson, M.D., Petrovskyy, D., Geiger, S. (2020). *Smart modelling of geologic stratigraphy concepts using sketches*. Paper presented at STAG2020 conference on Smart Tools and Applications in Graphics, November 12-13.

Deng, H., Stauffer, P. H., Dai, Z., Jiao, Z., & Surdam, R. C. (2012). Simulation of industrial-scale CO2 storage: Multi-scale heterogeneity and its impacts on storage capacity, injectivity and leakage. *International Journal of Greenhouse Gas Control, 10*, 397-418. https://doi.org/10.1016/j.ijggc.2012.07.003

Denver, L. E., & Phillips, D. C. (1990). Stratigraphic geocellular modeling. *Geobyte, 5*(1), 45-47.

Deveugle, P. E. K., Jackson, M. D., Hampson, G. J., Stewart, J., Clough, M. D., Ehighebolo, T., et al. (2014). A comparative study of reservoir modeling techniques and their impact on predicted performance of fluvial-dominated deltaic reservoirs. *AAPG Bulletin, 98*(4), 729-763. https://doi.org/10.1306/08281313035

Dockrill, B., & Shipton, Z. K. (2010). Structural controls on leakage from a natural CO_2 geologic storage site: Central Utah, U.S.A. *Journal of Structural Geology, 32*(11), 1768-1782. Article. https://doi.org/10.1016/j.jsg.2010.01.007

Doelling, H. H., Ross, M. L., & Mulvey, W. E. (2002). *Geologic map of the Moab 7.5' quadrangle, Grand county, Utah* (Vol. Map 181): Utah Geological Survey.

Duchon, J. (1977). *Splines minimizing rotation-invariant semi-norms in Sobolev spaces*, Berlin, Heidelberg.

Fahad Al-Ajmi, H., Keller, M., Hinderer, M., & Filomena, C. M. (2015). Lithofacies, depositional environments and stratigraphic architecture of the Wajid Group outcrops in southern Saudi Arabia. *GeoArabia, 20*(1), 49-94.

Feyen, L., & Caers, J. (2006). Quantifying geological uncertainty for flow and transport modeling in multi-modal heterogeneous formations. *Advances in Water Resources, 29*(6), 912-929. https://doi.org/10.1016/j.advwatres.2005.08.002

Foxford, K. A., Garden, I. R., Guscott, S. C., Burley, S. D., Lewis, J. J. M., Walsh, J. J., & Watterson, J. (1996). The field geology of the Moab Fault. In A. C. Huffman, W. R. Lund, & L. H. Godwin (Eds.), *Geology and Resources of the Paradox Basin* (Vol. 25, pp. 266-283): Utah Geological Association Guidebook.

Frery, E., Gratier, J.-P., Ellouz-Zimmerman, N., Loiselet, C., Braun, J., Deschamps, P., et al. (2015). Evolution of fault permeability during episodic fluid circulation: Evidence for the effects of fluid–rock interactions from travertine studies (Utah–USA). *Tectonophysics, 651-652*, 121-137. https://doi.org/10.1016/j.tecto.2015.03.018

Geiger, S., Matthäi, S. K., Niessner, J., & Helmig, R. (2009). Black-oil simulations for three-component, three-phase flow in fractured porous media. *SPE Journal, 14*(2), 338-354. https://doi.org/10.2118/107485-PA

Gershenzon, N. I., Ritzi Jr., R. W., Dominic, D. F., Soltanian, M., Mehnert, E., & Okwen, R. T. (2015). Influence of small-scale fluvial architecture on CO2 trapping processes in deep brine reservoirs. *Water Resources Research, 51*(10), 8240-8256. https://doi.org/10.1002/2015wr017638

Graham, G. H., Jackson, M. D., & Hampson, G. J. (2015). Three-dimensional modeling of clinoforms in shallow-marine reservoirs: Part 2. Impact on fluid flow and hydrocarbon recovery in fluvial-dominated deltaic reservoirs. *AAPG Bulletin, 99*(6), 1049-1080. https://doi.org/10.1306/01191513191

Graham, M. T., MacAllister, D., Vinogradov, J., Jackson, M. D., & Butler, A. P. (2018). Self-potential as a predictor of seawater Intrusion in coastal groundwater boreholes. *Water Resources Research, 54*(9), 6055-6071. https://doi.org/10.1029/2018wr022972

Hamilton, D. E., & Jones, T. A. (1992). *Computer modeling of geologic surfaces and volumes*: AAPG, Computer Applications in Geology, No 1.

Hampson, G. J., & Howell, J. A. (2005). Sedimentologic and geomorphic characterization of ancient wave-dominated deltaic shorelines: Upper Cretaceous Blackhawk Formation, Book Cliffs, Utah, USA. In L. Giosan & J. P. Bhattacharya (Eds.), *River deltas - concepts, models and examples* (Vol. 83, pp. 133-154): Society for Sedimentary Geology (SEPM) Special Publication. https://doi.org/10.2110/pec.05.83.0131

Huysmans, M., & Dassargues, A. (2011). Direct multiple-point geostatistical simulation of edge properties for modeling thin irregularly shaped surfaces. *Mathematical Geosciences, 43*(5), 521. https://doi.org/10.1007/s11004-011-9336-7

Huysmans, M., Peeters, L., Moermans, G., & Dassargues, A. (2008). Relating small-scale sedimentary structures and permeability in a cross-bedded aquifer. *Journal of Hydrology, 361*, 41-51.

Ingebritsen, S. E., Geiger, S., Hurwitz, S., & Driesner, T. (2010). Numerical simulation of magmatic hydrothermal systems. *Reviews of Geophysics, 48*(1). https://doi.org/10.1029/2009rg000287

Jackson, M. D., Gomes, J. L. M. A., Mostaghimi, P., Percival, J. R., Tollit, B. S., Pavlidis, D., et al. (2013a). *Reservoir modeling for flow simulation using surfaces, adaptive unstructured meshes, and control-volume-finite-element methods*. Paper presented at the 2013 SPE Reservoir Simulation Symposium, Feb 18-20, The Woodlands, TX, USA.

Jackson, M. D., Hampson, G. J., Rood, D., Geiger, S., Zhang, Z., Sousa, M. C., et al. (2015a). *Rapid Reservoir Modeling: prototyping of reservoir models, well trajectories and development options using an intuitive, sketch-based interface*. Paper presented at the SPE Reservoir Simulation Symposium, Houston, Texas, USA. https://doi.org/10.2118/173237-MS

Jackson, M. D., Hampson, G. J., Saunders, J. H., El-Sheikh, A., Graham, G. H., & Massart, B. Y. G. (2013b). Surface-based reservoir modelling for flow simulation. *Geological Society, London, Special Publications, 387*(1), 271-292. https://doi.org/10.1144/sp387.2

Jackson, M. D., Hampson, G. J., & Sech, R. P. (2009). Three-dimensional modeling of a shoreface-shelf parasequence reservoir analog: Part 2. Geologic controls on fluid flow and hydrocarbon recovery. *AAPG Bulletin, 93*(9), 1183-1208. https://doi.org/10.1306/05110908145

Jackson, M. D., Percival, J., Mostaghimi, P., Tollit, B., Pavlidis, D., Pain, C., et al. (2015b). Reservoir modeling for flow simulation by use of surfaces, adaptive unstructured meshes, and an overlapping-control-

volume finite-element method. *SPE Reservoir Evaluation & Engineering, 18*(2). https://doi.org/10.2118/163633-PA

Jackson, M. D., Yoshida, S., Muggeridge, A. H., & Johnson, H. D. (2005). Three-dimensional reservoir characterization and flow simulation of heterolithic tidal sandstones. *AAPG Bulletin, 89*(4), 507-528. https://doi.org/10.1306/11230404036

Jacquemyn, C., Jackson, M. D., & Hampson, G. J. (2019). Surface-based geological reservoir modelling using grid-free NURBS curves and surfaces. *Mathematical Geosciences, 51*(1), 1-28. https://doi.org/10.1007/s11004-018-9764-8

Janković, I., Fiori, A., & Dagan, G. (2006). Modeling flow and transport in highly heterogeneous three-dimensional aquifers: Ergodicity, Gaussianity, and anomalous behavior—1. Conceptual issues and numerical simulations. *Water Resources Research, 42*(6). https://doi.org/10.1029/2005wr004734

Kamola, D. L., & Huntoon, J. E. (1995). Repetitive stratal patterns in a foreland basin sandstone and their possible tectonic significance. *Geology, 23*(2), 177-180. https://doi.org/10.1130/0091-7613(1995)023<0177:Rspiaf>2.3.Co;2

Kamola, D. L., & Van Wagoner, J. C. (1995). Stratigraphy and facies architecture or parasequences with examples from the Spring Canyon Member, Blackhawk Formation, Utah. In J. C. Van Wagoner & G. T. Bertram (Eds.), *Sequence stratigraphy of foreland basin deposits* (Vol. 64, pp. 27-54): AAPG.

Koltermann, C. E., & Gorelick, S. M. (1996). Heterogeneity in Sedimentary Deposits: A Review of Structure-Imitating, Process-Imitating, and Descriptive Approaches. *Water Resources Research, 32*(9), 2617-2658. https://doi.org/10.1029/96wr00025

Lemon, A. M., & Jones, N. L. (2003). Building solid models from boreholes and user-defined cross-sections. *Computers & Geosciences, 29*(5), 547-555. https://doi.org/10.1016/S0098-3004(03)00051-7

Lidal, E. M., Patel, D., Bendiksen, M., Langeland, T., & Viola, I. (2013). *Rapid sketch-based 3D modeling of geology*. Paper presented at the Workshop on visualisation in environmental sciences (EnvirVis).

Linde, N., Renard, P., Mukerji, T., & Caers, J. (2015). Geological realism in hydrogeological and geophysical inverse modeling: A review. *Advances in Water Resources, 86*, 86-101. https://doi.org/10.1016/j.advwatres.2015.09.019

MacDonald, A. C., & Aasen, J. O. (1994). A prototype procedure for stochastic modeling of facies tract distribution in shoreface reservoirs. In J. M. Yarus & R. L. Chambers (Eds.), *Computer Applications 3: Stochastic Modeling and Geostatistics* (pp. 91-108): AAPG.

MacDonald, A. C., Fält, L. M., & Hektoen, A.-L. (1998). Stochastic modeling of incised valley geometries. *AAPG Bulletin, 82*(6), 1156-1172. https://doi.org/10.1306/1d9bca25-172d-11d7-8645000102c1865d

March, R., Doster, F., & Geiger, S. (2018). Assessment of CO_2 storage potential in naturally fractured reservoirs with dual-porosity models. *Water Resources Research, 54*(3), 1650-1668. https://doi.org/10.1002/2017wr022159

Massart, B. Y. G., Jackson, M. D., Hampson, G. J., & Johnson, H. D. (2016a). Effective flow properties of heterolithic, cross-bedded tidal sandstones: Part 2. Flow simulation. *AAPG Bulletin, 100*(5), 723-742. https://doi.org/10.1306/02011614222

Massart, B. Y. G., Jackson, M. D., Hampson, G. J., Johnson, H. D., Legler, B., & Jackson, C. A.-L. (2016b). Effective flow properties of heterolithic, cross-bedded tidal sandstones: Part 1. Surface-based modeling. *AAPG Bulletin, 100*(5), 697-721. https://doi.org/10.1306/02011614221

Matthäi, S. K., Geiger, S., Roberts, S. G., Paluszny, A., Belayneh, M., Burri, A., et al. (2007). Numerical simulation of multi-phase fluid flow in structurally complex reservoirs. *Geological Society, London, Special Publications, 292*(1), 405-429. https://doi.org/10.1144/sp292.22

Matthai, S. K., Mezentsev, A. A., & Belayneh, M. (2007). Finite element - node-centered finite-volume two-phase-flow experiments with fractured rock represented by unstructured hybrid-element meshes. *SPE Reservoir Evaluation & Engineering, 10*(6), 740-756. https://doi.org/10.2118/93341-PA

Mayo, A. L., Morris, T. H., Peltier, S., Petersen, E. C., Payne, K., Holman, L. S., et al. (2003). Active and inactive groundwater flow systems: Evidence from a stratified, mountainous terrain. *GSA Bulletin, 115*(12), 1456-1472. https://doi.org/10.1130/b25145.1

Miller, C. T., Christakos, G., Imhoff, P. T., McBride, J. F., Pedit, J. A., & Trangenstein, J. A. (1998). Multiphase flow and transport modeling in heterogeneous porous media: challenges and approaches. *Advances in Water Resources, 21*(2), 77-120. https://doi.org/10.1016/S0309-1708(96)00036-X

Narcowich, F. J., & Ward, J. D. (1994). Generalized Hermite Interpolation Via Matrix-Valued Conditionally Positive Definite Functions. *Mathematics of Computation, 63*(208), 661-687. https://doi.org/10.2307/2153288

Natali, M., Klausen, T. G., & Patel, D. (2014a). Sketch-based modelling and visualization of geological deposition. *Computers & Geosciences, 67*, 40-48. https://doi.org/10.1016/j.cageo.2014.02.010

Natali, M., Parulek, J., & Patel, D. (2014b). *Rapid modelling of interactive geological illustrations with faults and compaction*. Paper presented at the Proceedings of the 30th Spring Conference on Computer Graphics, Smolenice, Slovakia. 10.1145/2643188.2643201

O'Sullivan, M. J., Pruess, K., & Lippmann, M. J. (2001). State of the art of geothermal reservoir simulation. *Geothermics, 30*(4), 395-429. https://doi.org/10.1016/S0375-6505(01)00005-0

Olsen, L., Samavati, F. F., & Jorge, J. A. (2011). NaturaSketch: modeling from images and natural sketches. *IEEE Computer Graphics and Applications, 31*(6), 24-34. https://doi.org/10.1109/MCG.2011.84

Olsen, L., Samavati, F. F., Sousa, M. C., & Jorge, J. A. (2009). Sketch-based modeling: A survey. *Computers & Graphics, 33*(1), 85-103. https://doi.org/10.1016/j.cag.2008.09.013

Pereira, T., Brazil, E. V., Macêdo, I., Costa Sousa, M., de Figueiredo, L. H., & Velho, L. (2011). Sketch-based warping of RGBN images. *Graphical Models, 73*(4), 97-110. https://doi.org/10.1016/j.gmod.2010.11.001

Pyrcz, M. J., Catuneanu, O., & Deutsch, C. V. (2005). Stochastic surface-based modeling of turbidite lobes. *AAPG Bulletin, 89*(2), 177-191. https://doi.org/10.1306/09220403112

Refsgaard, J. C., Christensen, S., Sonnenborg, T. O., Seifert, D., Højberg, A. L., & Troldborg, L. (2012). Review of strategies for handling geological uncertainty in groundwater flow and transport modeling. *Advances in Water Resources, 36*, 36-50. https://doi.org/10.1016/j.advwatres.2011.04.006

Ronayne, M. J., Gorelick, S. M., & Caers, J. (2008). Identifying discrete geologic structures that produce anomalous hydraulic response: An inverse modeling approach. *Water Resources Research, 44*(8). https://doi.org/10.1029/2007wr006635

Ronayne, M. J., Gorelick, S. M., & Zheng, C. (2010). Geological modeling of submeter scale heterogeneity and its influence on tracer transport in a fluvial aquifer. *Water Resources Research, 46*(10). https://doi.org/10.1029/2010wr009348

Ruiu, J., Caumon, G., & Viseur, S. (2016). Modeling channel forms and related sedimentary objects using a boundary representation based on non-uniform rational B-splines. *Mathematical Geosciences, 48*(3), 259-284. journal article. https://doi.org/10.1007/s11004-015-9629-3

Sech, R. P., Jackson, M. D., & Hampson, G. J. (2009). Three-dimensional modeling of a shoreface-shelf parasequence reservoir analog: Part 1. Surface-based modeling to capture high-resolution facies architecture. *AAPG Bulletin, 93*(9), 1155-1181. https://doi.org/10.1306/05110908144

Shah, J. J., Vargas-Hernandez, N., Summers, J. D., & Kulkarni, S. (2001). Collaborative sketching (C-Sketch) - an idea generation technique for engineering design. *The Journal of Creative Behavior, 35*(3), 168-198. https://doi.org/10.1002/j.2162-6057.2001.tb01045.x

Shamshiri, H., & Jafarpour, B. (2012). Controlled CO_2 injection into heterogeneous geologic formations for improved solubility and residual trapping. *Water Resources Research, 48*(2). https://doi.org/10.1029/2011wr010455

Sommer, W., Valstar, J., van Gaans, P., Grotenhuis, T., & Rijnaarts, H. (2013). The impact of aquifer heterogeneity on the performance of aquifer thermal energy storage. *Water Resources Research, 49*(12), 8128-8138. https://doi.org/10.1002/2013wr013677

Strebelle, S. (2006). Sequential simulation for modeling geological structures from training images. In T. C. Coburn, J. M. Yarus, & R. L. Chambers (Eds.), *Stochastic modeling and geostatistics: Principles, methods and case studies - Volume II*: AAPG Computer Applications in Geology 5.

Sun, A. Y., Ritzi, R. W., & Sims, D. W. (2008). Characterization and modeling of spatial variability in a complex alluvial aquifer: Implications on solute transport. *Water Resources Research, 44*(4). https://doi.org/10.1029/2007wr006119

Taylor, C. B., Trompetter, V. J., Brown, L. J., & Bekesi, G. (2001). The Manawatu aquifers, North Island, New Zealand: Clarification of hydrogeology using a multidisciplinary environmental tracer approach. *Hydrological Processes, 15*(17), 3269-3286. https://doi.org/10.1002/hyp.272

Torabi, A., Ellingsen, T. S. S., Johannessen, M. U., Alaei, B., Rotevatn, A., & Chiarella, D. (2019). Fault zone architecture and its scaling laws: where does the damage zone start and stop? *Geological Society, London, Special Publications, 496*, SP496-2018-2151. https://doi.org/10.1144/sp496-2018-151

Wendland, H., & Rieger, C. (2005). Approximate interpolation with applications to selecting smoothing parameters. *Numerische Mathematik, 101*(4), 729-748. https://doi.org/10.1007/s00211-005-0637-y

White, C. D., & Barton, M. D. (1999). Translating outcrop data to flow models, with applications to the Ferron Sandstone. *SPE Reservoir Evaluation & Engineering, 2*(4), 341-350. https://doi.org/10.2118/57482-PA

White, C. D., Willis, B. J., Dutton, S. P., Bhattacharya, J. P., & Narayanan, K. (2004). Sedimentology, statistics, and flow behavior for a tide-influenced deltaic sandstone, Frontier Formation, Wyoming, United States. In G. M. Grammer, P. M. Harris, & G. P. Eberli (Eds.), *Integration of outcrop and modern analogs in reservoir modeling* (Vol. 80, pp. 129-152): AAPG Memoir.

Willis, B. J., & White, C. D. (2000). Quantitative Outcrop Data for Flow Simulation. *Journal of Sedimentary Research, 70*(4), 788-802. https://doi.org/10.1306/2dc40938-0e47-11d7-8643000102c1865d

Yao, T., Calvert, C., Bishop, G., Jones, T., Ma, Y., & Foreman, L. (2005). Spectral component geologic modeling: a new technology for integrating seismic information at the correct scale. In O. Leuangthong & C. V. Deutsch (Eds.), *Geostatistics Banff 2004* (pp. 23-33). Dordrecht: Springer Netherlands. https://doi.org/10.1007/978-1-4020-3610-1_3

Zhang, X., Pyrcz, M. J., & Deutsch, C. V. (2009). Stochastic surface modeling of deepwater depositional systems for improved reservoir models. *Journal of Petroleum Science and Engineering, 68*(1–2), 118-134. https://doi.org/10.1016/j.petrol.2009.06.019

Zhang, Z., Geiger, S., Rood, M., Jacquemyn, C., Jackson, M., Hampson, G., et al. (2017). A tracing algorithm for flow diagnostics on fully unstructured grids with multipoint flux approximation. https://doi.org/10.2118/182635-PA

Zhang, Z., Geiger, S., Rood, M., Jacquemyn, C., Jackson, M., Hampson, G., et al. (2020). Fast flow computation methods on unstructured tetrahedral meshes for rapid reservoir modelling. *Computational Geosciences, 24*(2), 641-661. https://doi.org/10.1007/s10596-019-09851-6

Zhang, Z., Geiger, S., Rood, M., Jacquemyn, C., Jackson, M. D., Hampson, G. J., & De Calvalho, F. M. (2018). Fast flow computation methods on unstructured tetrahedral meshes for Rapid Reservoir Modelling. *2018*(1), 1-15. https://doi.org/10.3997/2214-4609.201802241

Captions

Fig. 1. *Screenshot of the RRM research software interface, in which we have implemented the SBIM methods reported here. Screenshot illustrates the dataset used in Case Study I. Three main windows provide the views necessary to sketch a model, clockwise from top: (1) cross-section sketching window, (2) map-view sketching window, (3) 3D visualization window. In this example, the cross-section window has data loaded from five measured outcrop sections and boreholes. The position and orientation of the cross-section is visualized in transparent pink in the 3D window. The map-view sketching window has a map loaded showing the location of the cross-section, outcrop sections and boreholes. The leftmost panel lists all sketched surfaces and volumes (in stratigraphic order) and associated properties. As none are yet created, the panel is empty, but is populated as surfaces are sketched (Fig. 2).*

Fig. 2*. Sketched 3D model based on five measured outcrop sections and boreholes, illustrating the initial scenario SM1 for Case Study I. The parasequence boundaries (flooding surfaces) and facies boundaries are correlated by sketching in the cross-section window (top) displaying the measured outcrop sections and well logs (Fig. 1). These sketches are extruded along the trajectories sketched in map-view (bottom right). Facies boundaries in each parasequence are extruded using the green (lower parasequence), brown (middle parasequence), and yellow (upper parasequence) trajectories. A belt of flood tidal delta deposits (red facies in middle parasequence) follow the same map-view trajectory as the shoreface facies belts (brown trajectory for middle parasequence). The tide-influenced channelised sandbody (red facies in upper parasequence) follows the red trajectory on the map-view. The 3D model was sketched in less than 10 minutes (screen recording available in supplementary materials).*

Fig. 3*. Examples of different sketching procedures for initial interpretation model SM1. In all four sketching procedures, the surfaces are sketched in different order using different combinations of the operators but all result in the same 3D model (Fig. 2). (a-d) Hierarchical sketching procedure #1 first delineates the parasequences, which are then successively filled in with facies-bounding surfaces. A screen-recording of this procedure is available in supplementary material. e-h) Sketching procedure #2 sketches in approximately stratigraphic order starting from the base surface and sketches the facies-bounding surfaces in the lower parasequence prior to sketching the middle and upper parasequence boundaries. (i-l) Sketching procedure #3 sketches from top to bottom, starting with the facies boundaries of*

the upper parasequence, and sequentially working down to the basal surface. (m-p) Sketching procedure #4 takes a less organised approach, starting by correlating some of the facies-bounding surfaces in the middle of the sections. A logical interpretive order only appears when the middle parasequence is identified and is then truncated by top and base parasequence-bounding surfaces. The four procedures shown here are not exhaustive, as many other orders of sketching could be applied.

***Fig. 4**. 3D perspective views of the initial model SM1 for case study I. a) full 3D model. b) Tide-influenced channelised sandbody in the upper parasequence cuts into underlying foreshore and upper shoreface facies belts. c) Top view of middle parasequence. d-e) View of flood tidal delta deposits that form a continuous facies belt running parallel to depositional strike, up-dip of the upper-shoreface deposits. f) Top view of the lower parasequence.*

***Fig. 5**. Comparison of the initial model SM1 (left column) with models sketched for alternative scenarios SM2 to SM5 (right column) for Case Study I. Facies proportions are calculated for the different scenarios. a-b) Different down-dip extents of shoreface facies belts. c-d) Different orientation and rugosity of shoreface facies belts. e-f) Different geometry of flood tidal delta deposits. g-h) Different extent and geometry of tide-influenced channelised sandbodies, with associated changes in the orientation and curvature of shoreface facies belts. Each model scenario was sketched in less than 10 minutes.*

***Fig. 6**. Different approaches are possible to sketch the top bounding surface for the flood tidal delta deposits in the middle parasequence as isolated bodies. a-c) Geometry can be sketched in multiple horizontal planes, outlining contours. The apex of the geobody is sketched in plane a. The sketch in plane c corresponds to where the geobody pinches out on the underlying surface. One or more additional planes (e.g. plane b) can be added in between for extra control of the final geometry. d-f) An alternative approach to sketch flood tidal delta deposits is in vertical cross-sections, in strike or dip orientation. In (d- f) the flood tidal delta is sketched on vertical, strike-oriented cross-sections at a proximal, mid, and distal location through the deposits. (g-h) show the positions of the respective sketching planes a-f in the 3D model and the resulting geobodies.*

***Fig. 7**. Sketched 3D model based on a road-cut outcrop, illustrating the initial scenario NF1 for Case Study II. The top window shows the sketched interpretation of faults and bed boundaries on the outcrop, which is assumed to be a vertical cross-section. Bottom right window shows sketched map-view trajectories representing the fault strike in scenarios NF2 and NF3 (dashed blue lines); for scenario NF1, no strike orientation is defined and all*

sketched surfaces are simply extruded perpendicular to the vertical cross-section. Bottom left window shows the resulting 3D model, with the location of the vertical cross-section (top) shown in the centre of the model (dashed black line). The 3D model was sketched in less than 20 minutes (screen recording available in supplementary materials).

***Fig. 8**. Two different approaches to sketch the initial interpretation model NF1. (a-d) Sketch all faults (steps 1-13) before sketching the bed boundaries in each fault block (steps 14-76). (e-h) Combination of sketching some bed boundaries first (e.g. steps 1-7) and then sketching faults (steps 8-14) and adding detail within the newly created fault blocks (18-57).*

***Fig. 9**. Comparison of models sketched for three different scenarios of Case Study II from different perspectives. a-c) Initial scenario NF1 with linear synthetic and antithetic faults of parallel strike. d-f) Scenario NF2: Synthetic and antithetic faults no longer have parallel strike. This results in additional fault blocks being created (blue rectangles). g-i) Scenario NF3: Two fault blocks are added to NF2 (d and g: blue arrows; f and i: blue circles).*

***Fig. 10**. Screenshots of flow diagnostics output for modelled scenario SM5 (Fig. 5h). One vertical injector well (well 1) is placed in the northwest corner of the model, and two vertical producer wells in the south and northeast parts of the model (wells 2 and 3, respectively). a) Facies model, b) permeability, c) pressure distribution, and d) time-of-flight for tracer to reach the producer wells (threshold at 10 years), highlights flow through high-permeability facies (b) developed at specific stratigraphic levels and with variable lateral continuity.*

Figure 1

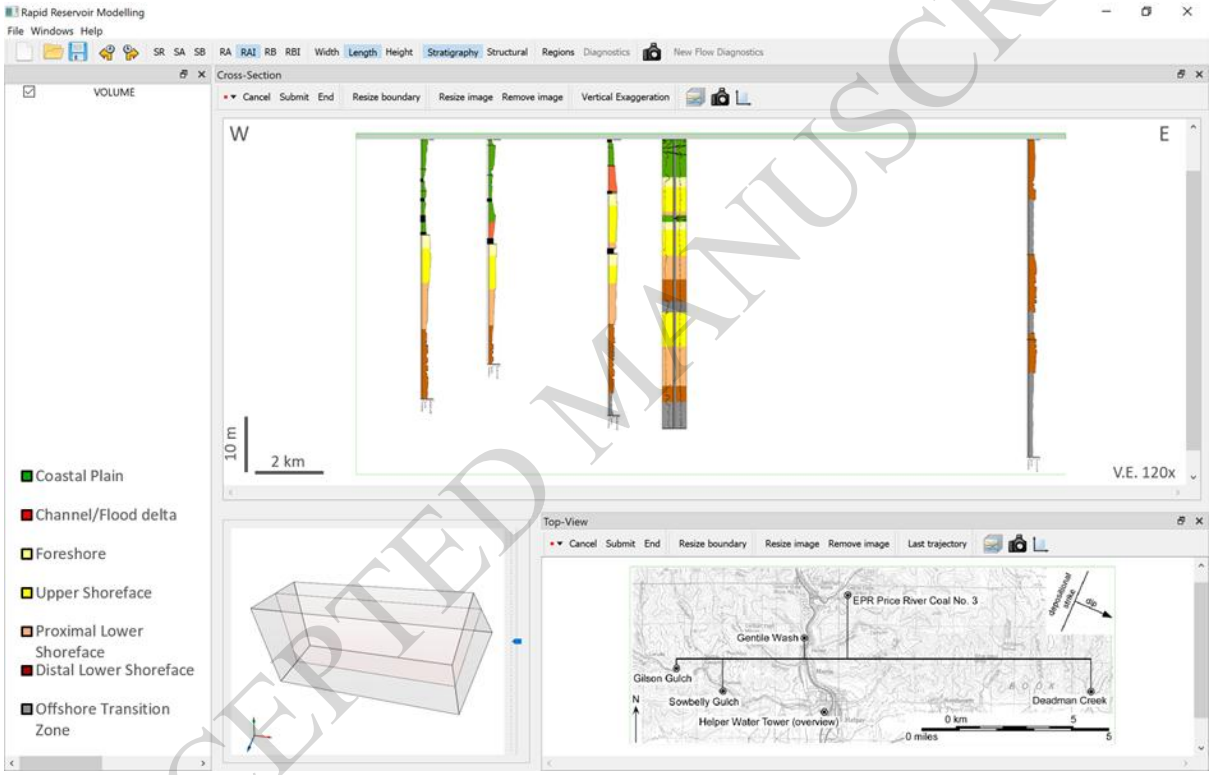

Figure 2

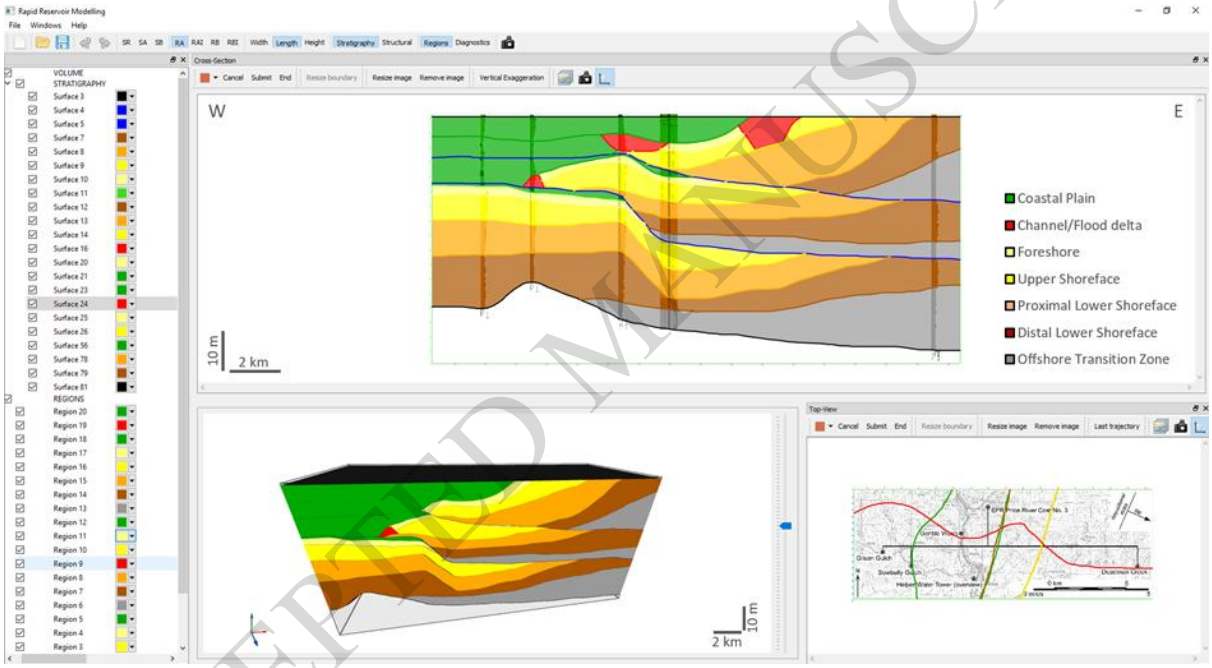

Figure 3

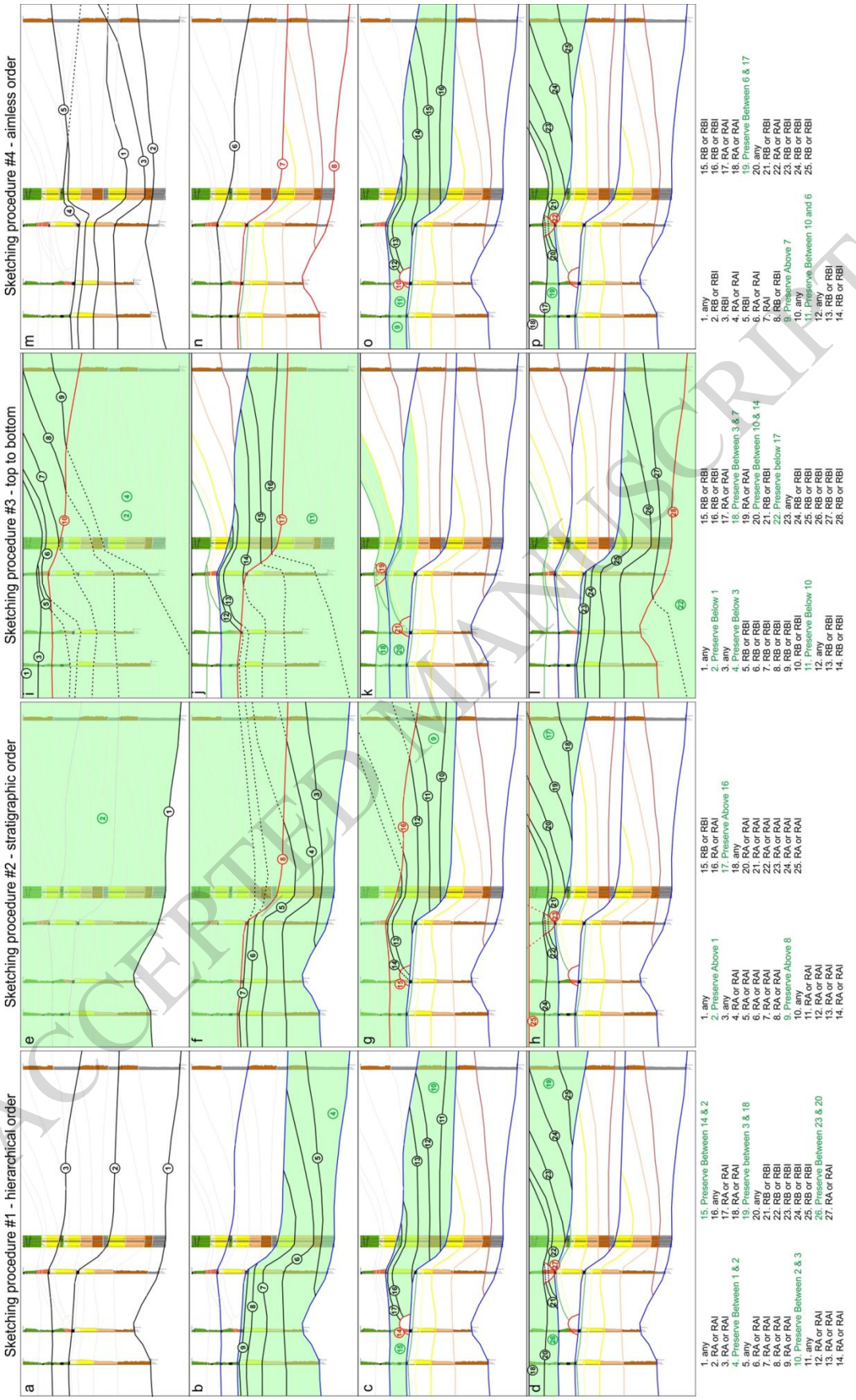

Figure 4

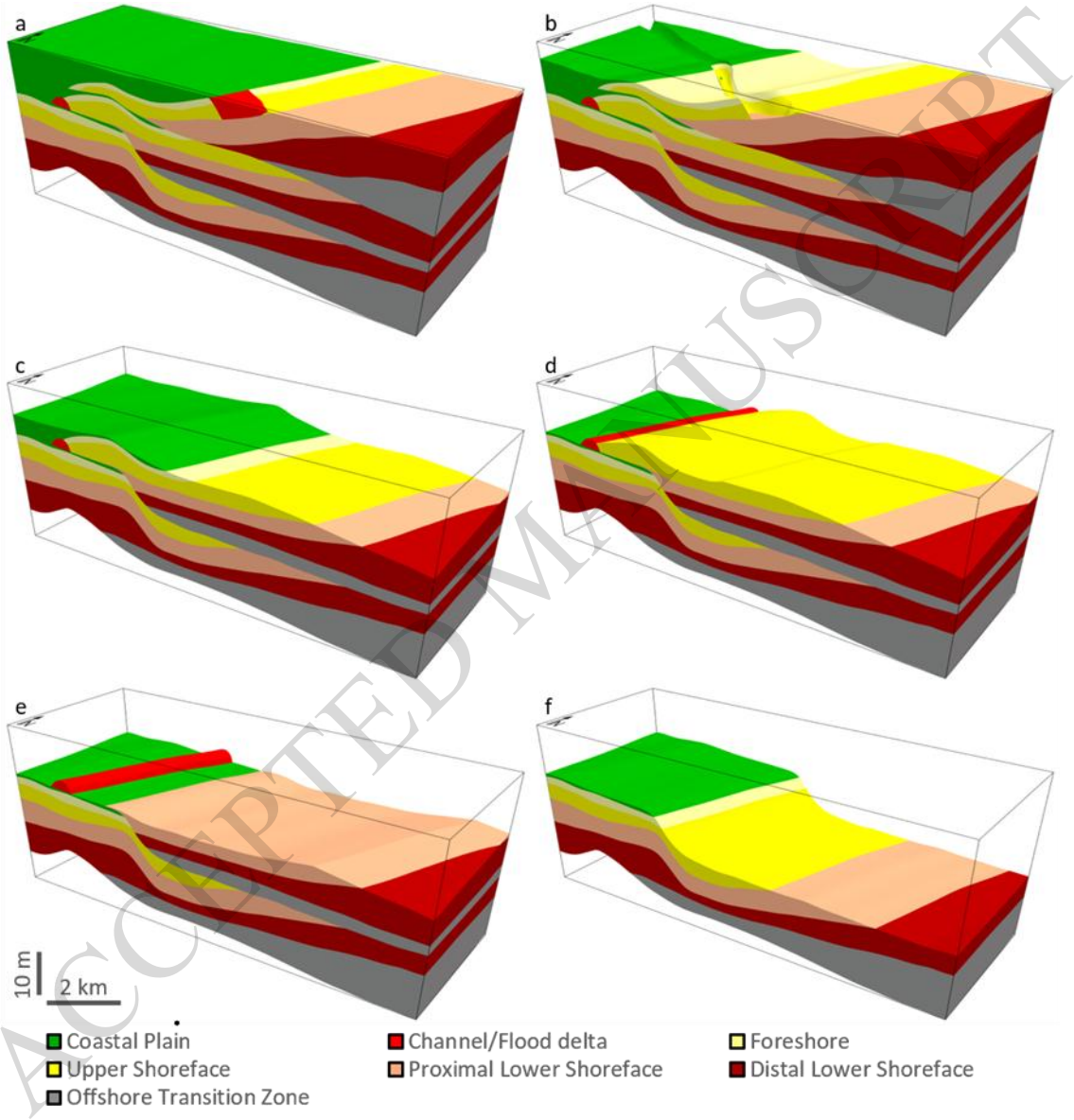

Figure 5

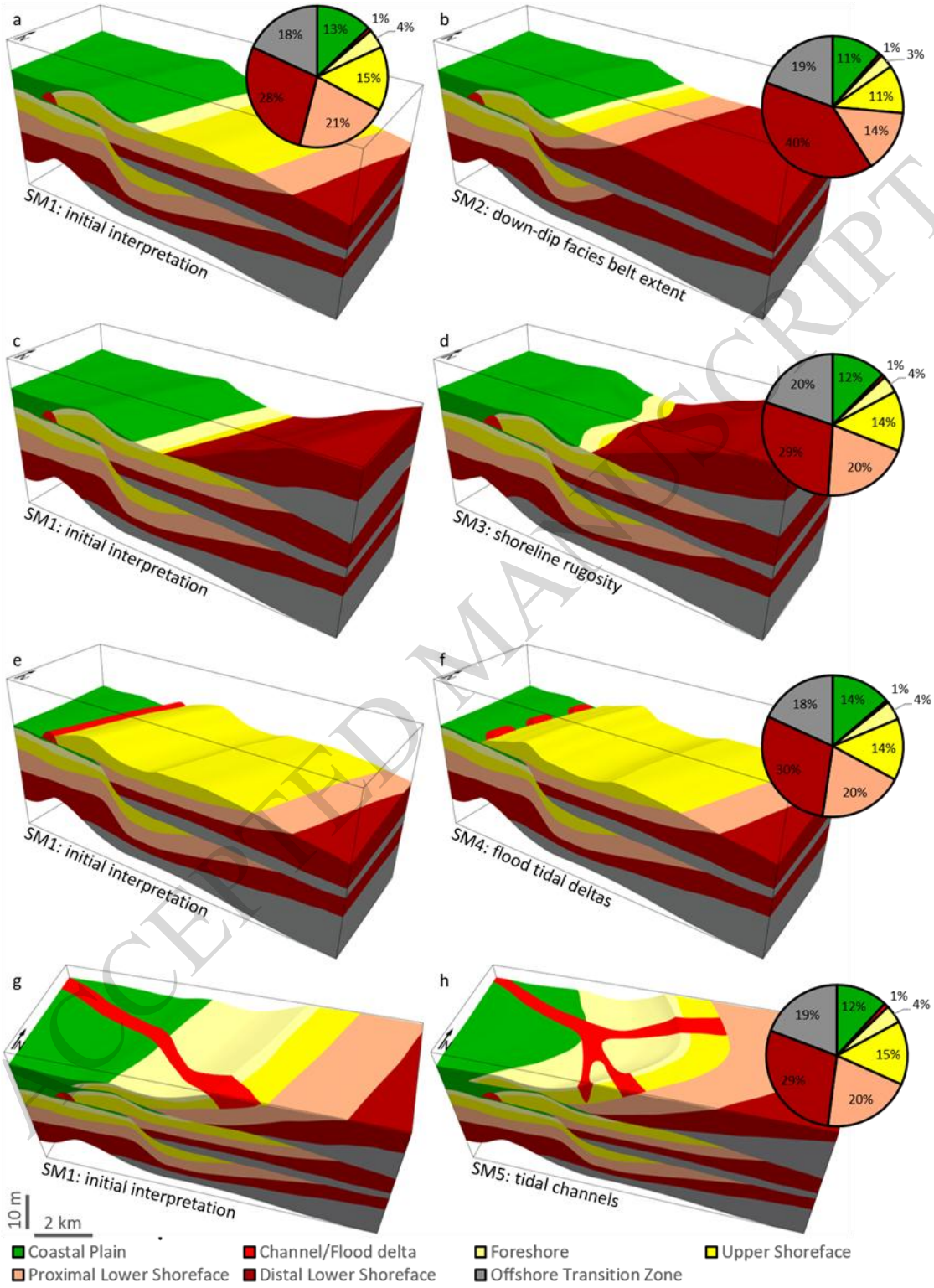

Figure 6

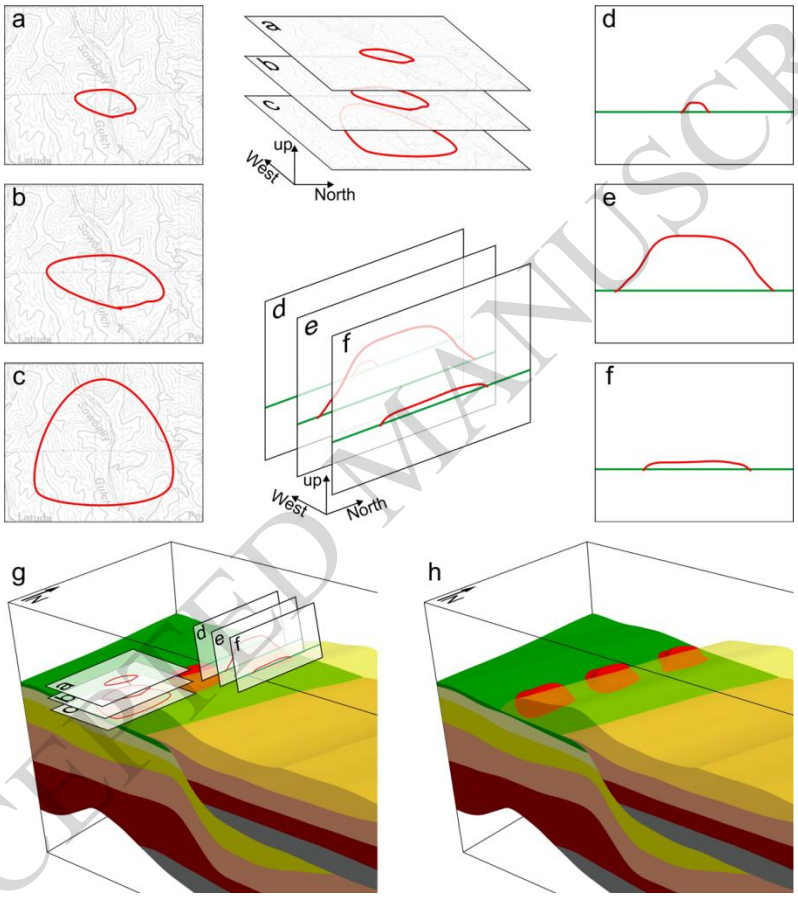

Figure 7

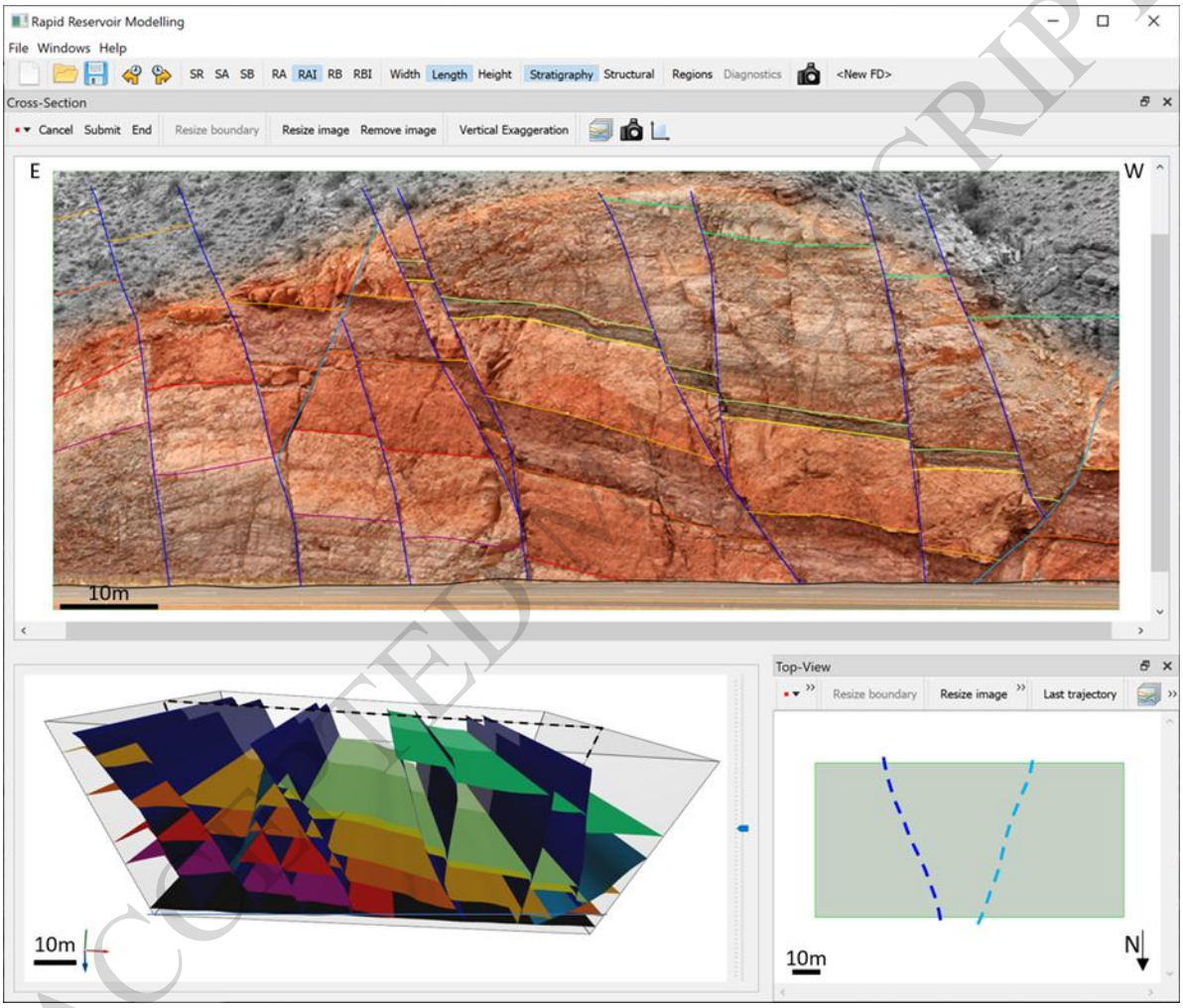

Figure 8

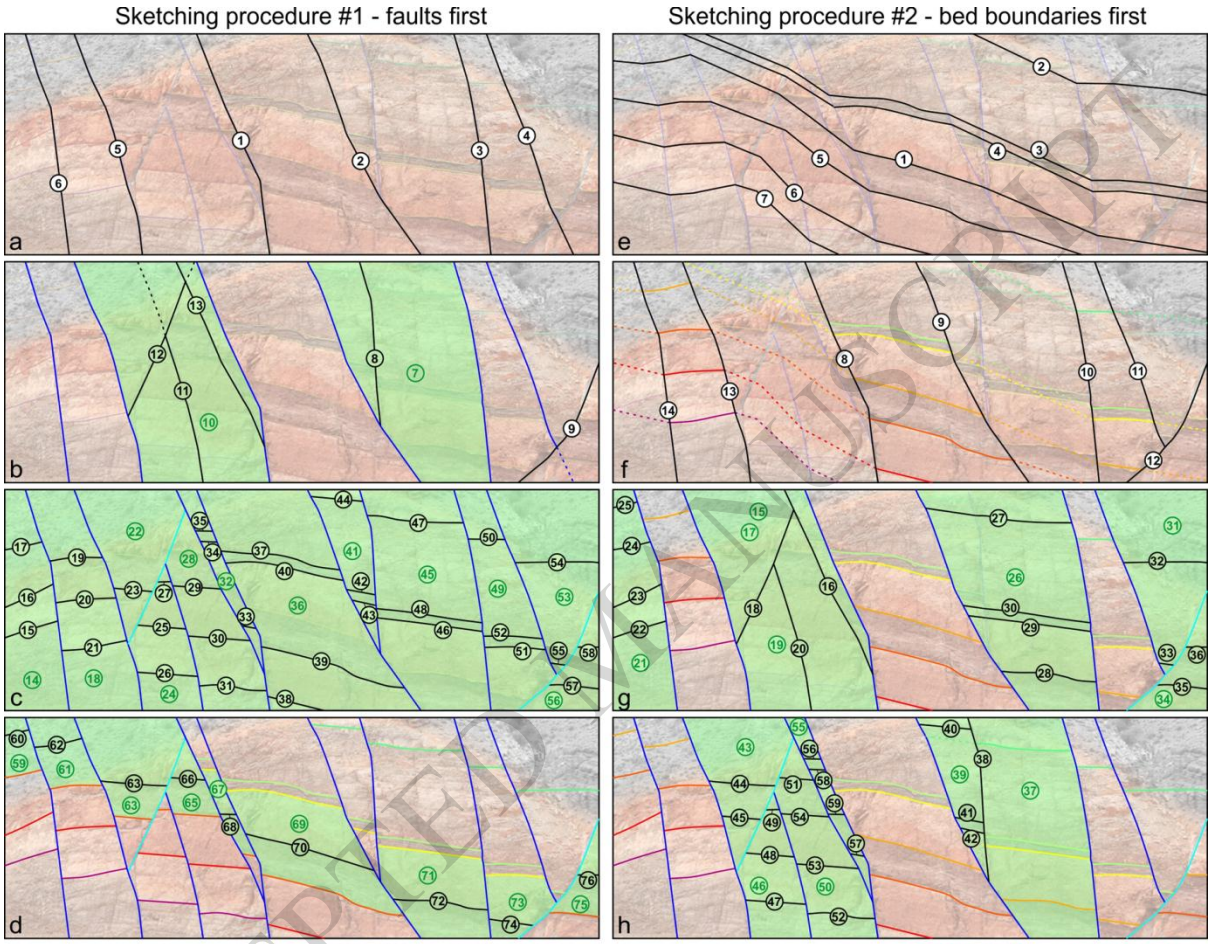

1. any
2. RA or RAI
3. RA or RAI
4. RA or RAI
5. RB or RBI
6. RB or RBI
7. PBW 2 & 3
8. any
9. RB or RBI
10. PBW 1 & 5
11. any
12. RA or RAI
13. RA or RAI
14. PB 6
15. any
16. RA or RAI
17. RA or RAI
18. PBW 5 & 6
19. any
20. any
21. RB or RBI
22. PBW 5 & 12
23. any
24. PBW 11 & 12
25. any
26. RB or RBI
27. RA or RAI
28. PBW 11 & 13
29. any
30. RB or RBI
31. RB or RBI
32. PBW 1 & 13
33. any
34. RA or RAI
35. RA or RAI
36. PBW 1 & 2
37. any
38. RB or RBI
39. RAI or RBI
40. RAI or RBI
41. PBW 2 & 8
42. any
43. RB or RBI
44. RA or RAI
45. PBW 3 & 8
46. any
47. RA or RAI
48. RAI or RBI
49. PBW 3 & 4
50. any
51. RA or RAI
52. RAI or RBI
53. PBW 4 & 9
54. any
55. RA or RAI
56. PB 9
57. any
58. RA or RAI
59. PA 17
60. any
61. PA 19
62. any
63. PA 23
64. any
65. PA 29
66. any
67. PBW 33 & 34
68. any
69. PBW 39 & 40
70. any
71. PB 46
72. any
73. PB 51
74. any
75. PA 57
76. any

1. any
2. RA or RAI
3. RAI or RBI
4. RAI or RBI
5. RA or RAI
6. RA or RAI
7. RA or RAI
8. RBI
9. RAI
10. RBI
11. RA or RAI
12. RB or RBI
13. RAI
14. RB or RBI
15. PBW 8 & 13
16. any
17. PBW 13 & 16
18. any
19. PBW 16 & 18
20. any
21. PB 14
22. any
23. RA or RAI
24. RA or RAI
25. RA or RAI
26. PBW 9 & 10
27. any
28. RA or RAI
29. RAI or RBI
30. RAI or RBI
31. PBW11 & 12
32. any
33. RB or RBI
34. PB 12
35. any
36. RA or RAI
37. PBW 9 & 10
38. RB or RBI
39. PBW 9 & 38
40. any
41. RB or RBI
42. RA or RBI
43. PBW 13 & 18
44. any
45. RB or RBI
46. PBW 18 & 20
47. any
48. RA or RAI
49. RA or RAI
50. PBW 16 & 20
51. any
52. RA or RAI
53. RAI or RBI
54. RAI or RBI
55. PBW 8 & 16
56. any
57. RA or RAI
58. RAI or RBI
59. RAI or RBI

Figure 9

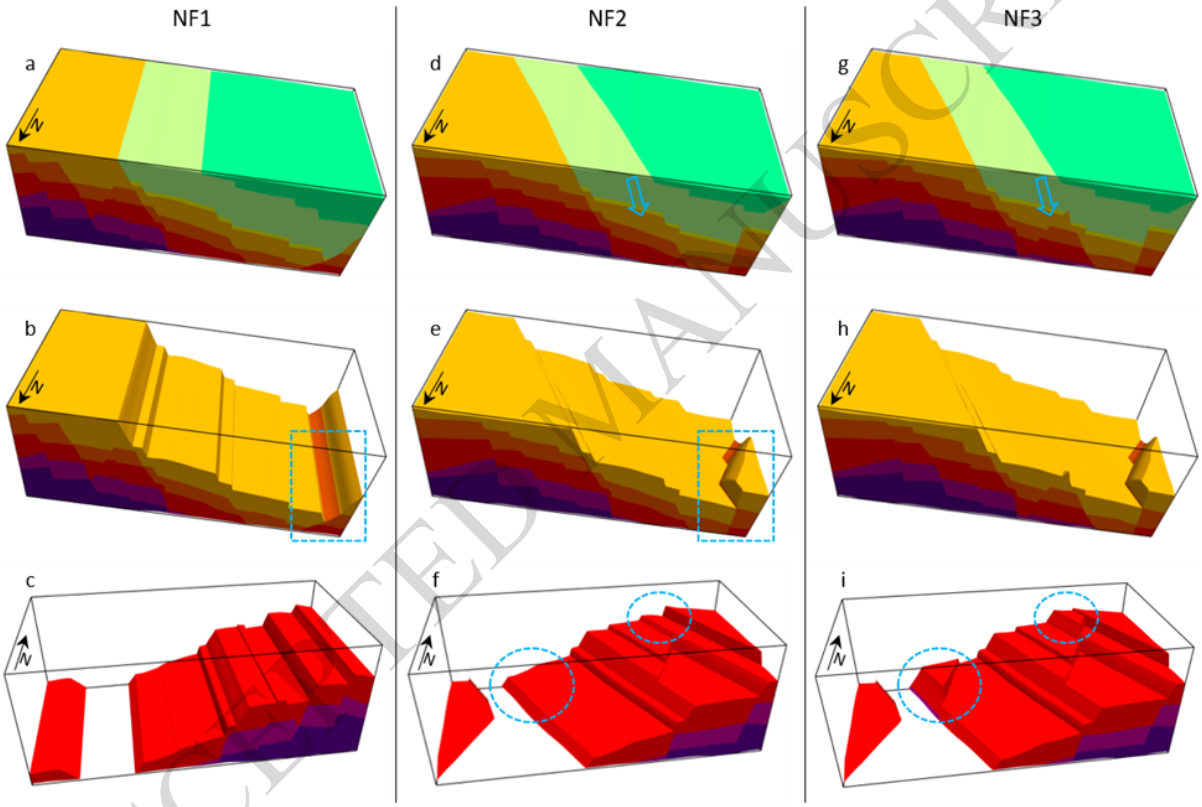

Figure 10